January 2012

Utility Of Apparent Diffusion Coefficients In The Evaluation Of Primary Central Nervous System Lymphoma

John Webster Gilbert
Yale School of Medicine, johngilbert2012@gmail.com

UTILITY OF APPARENT DIFFUSION COEFFICIENTS IN THE EVALUATION OF PRIMARY CENTRAL NERVOUS SYSTEM LYMPHOMA

A Thesis Submitted to the
Yale University School of Medicine
In Partial Fulfillment of the Requirements for the
Degree of Doctor of Medicine

By John Webster Gilbert

2012

Abstract

UTILITY OF APPARENT DIFFUSION COEFFICIENTS IN THE EVALUATION OF PRIMARY CENTRAL NERVOUS SYSTEM LYMPHOMA.

John W. Gilbert[1], Joachim M. Baehring[2], Susanne Barth[2], Ephraim P. Hochberg[3], Fred H. Hochberg[4], and Robert K. Fulbright (Sponsor)[1]

[1]Department of Diagnostic Radiology, Yale School of Medicine, New Haven, CT
[2]Departments of Neurology, Neurosurgery, and Internal Medicine, Yale School of Medicine, New Haven, CT
[3]Department of Internal Medicine, Massachusetts General Hospital, Boston, MA
[4]Pappas Center for Neuro-Oncology, Massachusetts General Hospital, Boston, MA

The characterization of primary central nervous system lymphoma (PCNSL) via noninvasive imaging modalities is essential for early diagnosis and differentiation from other brain lesions. Diffusion-weighted magnetic resonance imaging (DW-MRI), in which intensity of image contrast reflects diffusion of water molecules by Brownian motion, offers additional information beyond that obtained from conventional MRI. In this retrospective study from two institutions, quantitative region of interest (ROI) analysis was performed using parametric apparent diffusion coefficient (ADC) maps in immunocompetent patients with newly diagnosed PCNSL prior to corticosteroid use or other therapy. Mean ADC values and ratios were calculated for PCNSL lesions, peritumoral edema, and contralateral normal white matter. Quantitative DW-MRI analysis (n=12) revealed significant inter-group variance between the mean ADC of lesion, peritumoral region, and normal white matter. Tukey post-hoc comparison of the three groups indicate that the mean ADC of the peritumoral region is significantly different ($p<0.05$) from mean ADC of the lesion and normal white matter, while differences between mean ADC of the lesion and normal white matter were not statistically significant. A comprehensive review of prior investigations reporting ADC values in evaluation of PCNSL was also conducted. We found that restricted diffusion is a consistent imaging finding in immunocompetent PCNSL patients and a reliable surrogate marker of tumor cellularity; however, the ranges of ADC values reported for PCNSL varied between studies and also overlapped with ADC ranges reported for other brain tumors. Given the observed variability in ADC values, it is essential to consider DW-MRI data as an adjunct diagnostic tool interpretable only in the context of clinical presentation and conventional MRI data. Further prospective investigation enrolling patients prior to corticosteroid therapy will be necessary to obtain standardized pre-treatment ADC values.

Acknowledgements

First and foremost, I would like to thank my advisor Dr. Robert Fulbright for introducing me to this project. His radiological acumen, seemingly inexhaustible patience, and enthusiasm toward mentoring medical student “neuroradiology neophytes” such as myself are truly inspiring. My deep gratitude also to Dr. Baehring and his collaborators, who envisioned this study, coordinated an impressive patient cohort spanning two institutions, and gave me the opportunity to contribute to the project.

Data from this thesis are used in a recently submitted manuscript that includes (in addition to the quantitative ADC analysis reported here) descriptive findings in a comprehensive neuroimaging protocol including DW-MRI:

Baehring JM, Barth S, Gilbert JW, Hochberg E, Hochberg FH, Fulbright RK. Diffusion-weighted magnetic resonance imaging findings in primary central nervous system lymphoma.

Table of Contents

Introduction

Primary central nervous system lymphoma (PCNSL) is an aggressive extranodal non-Hodgkin (NHL) lymphoma that targets brain, vitreous body and optic nerves, leptomeninges, and spinal cord. (1-2) PCNSL accounts for approximately 2.4% of all primary CNS neoplasms by most recent estimates. (3) The incidence of PCNSL increased approximately threefold in the 1980s and early 1990s, with the rate of increase levelling off since then. (4-5) Individuals with congenital or acquired immunodeficiency such as HIV or immunosuppressive therapy after an organ transplant are predisposed to developing PCNSL, and it is believed that the reduction in rate of increase of PCNSL incidence is at least partially attributable to the introduction of highly active antiretroviral therapy (HAART) in the mid-1990s. (5) Nevertheless, incidence continues rise in both immunocompetent and immuncompromised populations, across all age groups and in both men and women. (6)

The clinical history of patients with PCNSL is variable. Most commonly, patients present with signs of a focal mass lesion, including evidence of increased intracranial pressure, seizures (more often in patients with AIDS), disturbances of vision, confusion, lethargy, memory loss, and neuropsychiatric manifestations. (7) Vague or unusual presenting complaints are also possible, e.g. a recent case report of fever of unknown origin as the sole presenting manifestation, (8) or panhypopituitarism and diabetes insipidus due to bilateral hypothalamic involvement. (9) A neurologic prodrome is sometimes seen up to years prior to diagnosis, which can include chronic vitritis (10) or multiple sclerosis. (11,12,13) Demyelinating

“sentinel” lesions that recede spontaneously up to months/years before the development of PCNSL have also been reported. (14-15) Whether these disorders reflect an early stage of malignancy heralding PCNSL or atypical polyclonal lymphoproliferations remains unclear. So-called “B” symptoms (fever, weight loss, night sweats) common in other forms of NHL are seldom seen except in the rare case of systemic dissemination.

For patients who present with acute symptoms of brain tumor, non-contrast computed tomography (CT) of the head is the initial test of choice, primarily as a screening tool to rule out immediately life-threatening intracranial pathology such as a herniation or bleed. (16) However, due to the poor soft tissue contrast of head CT, this imaging modality is not effective at discriminating subtle non-enhancing parenchymal changes. (17) Given the additional ionizing radiation exposure and the risk of contrast-induced hypersensitivity, head CT is reserved for initial acute evaluation due to its wide availability, speed, and relatively low cost.

For further evaluation of patients with suspected brain tumor, the most sensitive and specific diagnostic imaging modality is gadolinium contrast-enhanced magnetic resonance imaging (MRI). (2) Its advantages are numerous: superior anatomical detail, less risk of intolerance with gadolinium vs. iodinated contrast, no ionizing radiation, and flexible acquisition in multiple planes. The standard protocol includes contrast-enhanced T1 and fluid attenuated inversion recovery (FLAIR) sequences; T1 with contrast is well-suited for evaluating disruption of the blood-brain barrier with subsequent leakage of gadolinium, while FLAIR (a T2-weighted image in

which free water is attenuated) is excellent at identifying peritumoral edema and extent of tumor infiltration. (16,18)

Using these conventional MRI sequences, PCNSL typically presents in immunocompetent patients as homogenously enhancing solitary or multiple lesions, often in a periventricular location with spread along white matter tracts producing mild edema or mass effect. (19,20,21) Lesions are hypointense or hyperintense on T1-weighted images and roughly 40% are hyperintense T2-weighted signal by recent estimates. (22) However, in immunocompromised individuals T2 hyperintensity is more common, which has been show to correlate histologically with degree of intratumoral necrosis. (23) FLAIR sequence will demonstrate extensive perifocal edema with nonenhancing tumor area. In terms of distribution, a recent series of 100 immunocompetent PCNSL cases revealed lesions in cerebral hemisphere (38%), thalamus/basal ganglia (16%), corpus callosum (14%), periventricular region (12%), and cerebellum (9%). (24) Spinal cord or brainstem involvement, meningeal or ventricular enhancement, calcification and hemorrhage were uncommon.

The pattern of enhancement in PCNSL is variable, particularly in HIV/AIDS patients or other immunocompromised individuals in which multiple lesions and rim enhancement surrounding zones of central necrosis are more common (19). This creates a diagnostic dilemma in distinguishing PCNSL from another common AIDS-associated space-occupying lesion, CNS toxoplasmosis, which has a similar rim-enhancing appearance on MRI. (25) Diagnosis is further complicated by the empiric use of corticosteroids in the patient population, which can significantly alter the

appearance of PCNSL lesions by reducing contrast enhancement and brain edema and altering cellular morphology through a direct lymphocytotoxic effect. (26)

Given these diagnostic challenges, there is great interest in utilizing other noninvasive imaging modalities and/or biomarkers in order to better characterize PCNSL and differentiate it from other tumors. One such modality is diffusion-weighted MR imaging (DWI), in which intensity of image voxels reflects microscopic diffusion of water molecules in tissues by stochastic (Brownian) motion. (27) A brief technical review of DWI will now be presented to provide a theoretical framework for discussion of its clinical applications and rationale for use in PCNSL.

Basic Principles of Molecular Diffusion and Diffusion-Weighted Imaging

First described by Einstein in 1905, (28) the principle of Brownian motion states that molecules in a fluid medium diffuse randomly as a result of the thermal energy carried by those molecules. (27) Assuming a homogeneous medium of "free water," diffusion follows a three-dimensional Gaussian distribution with a variance $\sigma^2 = 2 * D * t$ where t = time allowed for diffusion and D = diffusion coefficient, which reflects size of molecules, temperature, and viscosity of a medium. (29) Biological tissues are far from homogeneous, however, and present obstacles to diffusion (cellular membranes, organelles, etc.) that result in anisotropic diffusion in a non-Gaussian pattern, particularly as diffusion distance increases. Diffusion MRI provides insight into microscopic tissue structure – and perturbations in that structure caused by pathologic states – by non-invasively recording diffusion of water molecules in vivo.

In conventional MRI techniques, a homogenous magnetic field is applied to stimulate precession of water hydrogen nuclei (protons) around an axis parallel to the direction of the magnetic field. The key difference of DWI is that a “dephasing” pulse field sequence consisting of two symmetrical gradient pulses is applied to introduce variance in magnetic strength. As early as 1950, Hahn discovered that in the presence of a heterogeneous magnetic field, protons spin so as to reduce signal intensity. (30) Precession rate of protons varies proportionally to magnet strength, in the same way that the precession rate of a gyroscope depends on the force of gravity. (31) Applying a pulsed field gradient in DWI thus alters the rate of precession of protons and leads to phase dispersion of their transverse magnetizations (xy component of net magnetization vector), which results in signal loss. (32) A “rephasing” radiofrequency (RF) pulse identical in direction but opposite in magnitude is applied to *refocus* this dispersion in between the gradient pulses. However, spins that have moved along the gradient axis in the interval between the application of the first and second gradient pulses will not be reset to their initial state; rather, a phase shift will occur relative to the hydrogen protons of immobile water molecules. This manifests as signal loss because the overall vectorial sum of the spin phases in a dispersed state is less than if they were all precessing synchronously.

The amount of signal loss can be predicted with the following equation originally described by Stejskal and Tanner in 1965:

$$\frac{S}{S_0} = e^{-\gamma^2 G^2 \delta^2 (\Delta - \delta/3) D} = e^{-bD}$$

(33)

where S is signal after pulsed field gradient application; S_0 is signal intensity prior to gradient application; γ is a constant termed the *gyromagnetic ratio*, representing the ratio of a proton nuclear magnetic dipole moment to its angular momentum—when multiplied by the magnetic field strength in Tesla (T), this represents the rate of proton nuclear precession known as the *Larmor frequency*; (34) G and δ are strength and duration of gradient pulse, respectively; Δ is time between application of two pulses; D is the diffusion coefficient; and *b*-value is a summary "diffusion-sensitizing factor" reflecting the overall strength of diffusion weighting. (33) A summary of the diffusion MR pulsed field gradient incorporated into a representative spin-echo sequence is provided in **Figure 1.**

According to Stejskal and Tanner's equation, four major variables can impact DWI signal intensity: time between application of the two gradients, strength and duration of gradient pulse applied, and the diffusion coefficient. It makes sense intuitively that signal intensity decreases as the amount of time between application of the two gradient pulses increases, because water molecules are allowed more time to diffuse; consequently, the phase refocusing pulse is less exact due to a larger displacement distribution of spins, which translates as signal attenuation. Signal intensity also varies proportionally with the strength and duration of the gradient pulse applied. These effects reflecting diffusion sensitization are summarized by the b-value. Finally, signal intensity varies according to the intrinsic rate of diffusion in tissues represented mathematically by the diffusion constant. Simply stated, faster diffusion results in larger phase shifts and greater signal loss.

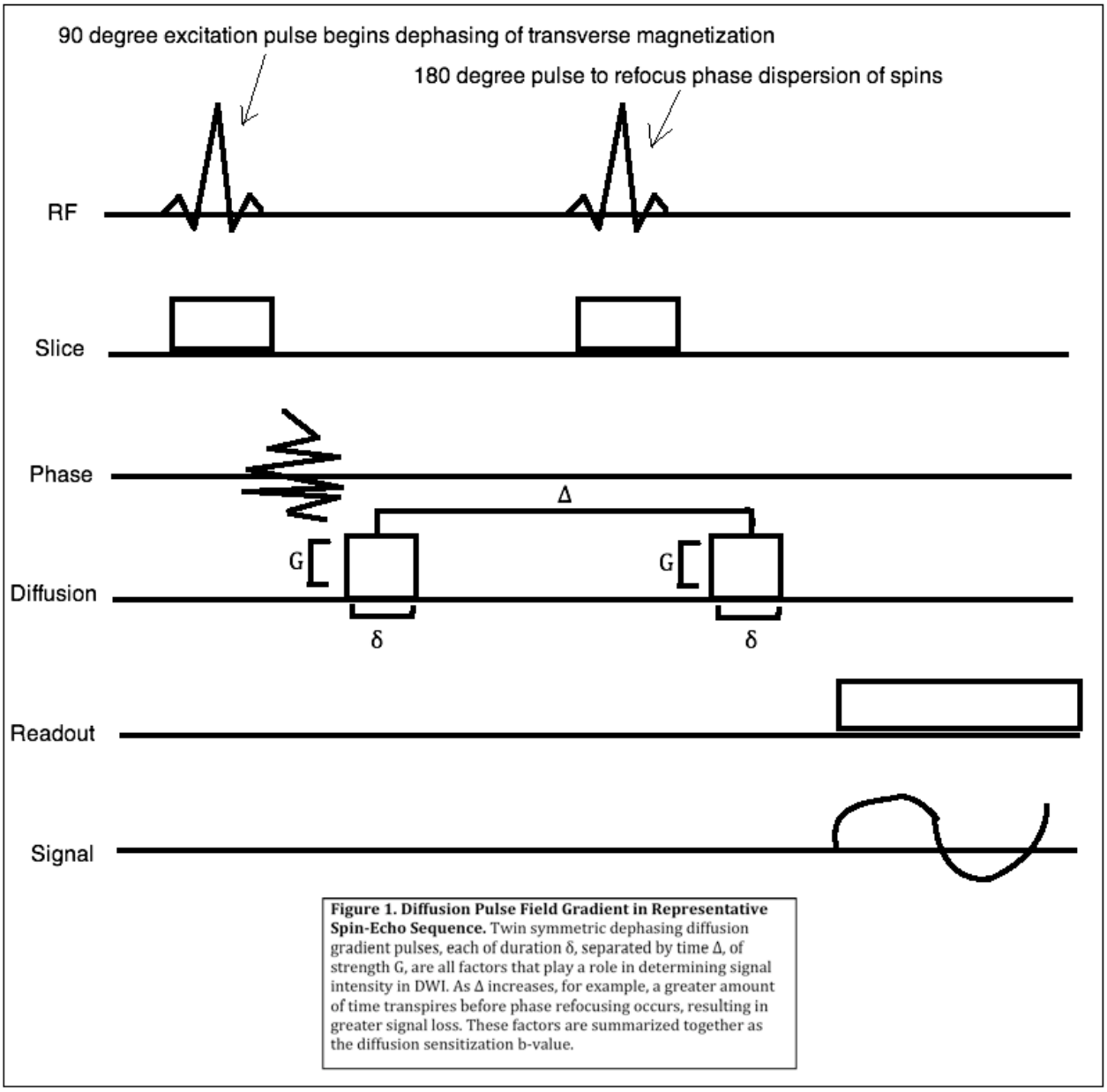

Figure 1. Diffusion Pulse Field Gradient in Representative Spin-Echo Sequence. Twin symmetric dephasing diffusion gradient pulses, each of duration δ, separated by time Δ, of strength G, are all factors that play a role in determining signal intensity in DWI. As Δ increases, for example, a greater amount of time transpires before phase refocusing occurs, resulting in greater signal loss. These factors are summarized together as the diffusion sensitization b-value.

Diffusion weighting can be used with many different imaging sequences but echo planar imaging (EPI) is often utilized because acquisition is rapid (typically in a single acquisition period of 25-100 msec) (35) and macroscopic motion artifacts (e.g. “ghosting,” “blurring”) due to patient motion, breathing, or pulsatile blood flow are consequently minimized. (36) Motion is a particular issue for diffusion MRI because the microscopic motion of interest that induces phase shifts in spins can easily be

confounded by macroscopic motion of the type described above. This would not necessarily be an issue if all spins experienced the same approximate displacement, but because each sequence is repeated several times, the aberrant macroscopic motion pattern is present in some runs but not others, resulting in the “ghosting” artifact. As is often unfortunately the case, however, the solution to this problem introduces problems all its own— EPI itself is prone to artifacts such as chemical shift and eddy currents produced when gradient pulses are switched on and off, and the magnetic field gradient generates a current through the conducting surfaces of the MRI scanner. (36)

Another important caveat is that diffusion-weighted images do *not* provide the most accurate indicator of the diffusion coefficient. This is because visual contrast on DWI is not solely b-value dependent, but also reflective of other weighting mechanisms (e.g. T2 relaxation). (31) In fact, when b-value = 0, the image sequence is simply that of a T2-weighted sequence which only reflects diffusion weighting once a pulsed field gradient is applied. A classic example of a problem in interpretation stemming from this issue is “T2 shine through” in which a hyperintensity on DWI may reflect T2 weighting and cannot be differentiated from true diffusion restriction. (36) In order to characterize water diffusion free of similar confounders, it was proposed that the physical diffusion coefficient be replaced by a statistical parameter, the apparent diffusion coefficient (ADC). (37) To calculate ADC, *b*-values from at least two acquisitions (typically b=0 and b=1000 s/mm^2) are plotted logarithmically against signal intensity, and the slope (i.e, rate of signal

decay) is deemed the diffusion constant, which can be mapped pixel-by-pixel to create a parametric ADC image map (**Figure 2**).

As a statistical parameter, ADC depends not only on intrinsic physical diffusion properties but also on other technical features such as diffusion time and voxel size; additionally, the scaling from voxels (usually on the order of a few cubic millimeters) results in an averaging or smoothing effect (36-38). How, then, do scientists and clinicians rationalize the fact that different portions within a single voxel may have significantly different diffusion properties? The parameterization and averaging has been likened to the efforts of meteorologists to describe natural atmospheric processes on a scale much larger than the local physical forces being approximated, forces that technical limitations prevent us from accurately measuring, whether it be diffusion in tissue microarchitecture or the microphysics of thunderstorms. (38) The underlying assumption is that as long as one can make reliable and informed predictions based on the data, the parameter need not reflect the physical environment with complete accuracy in order to remain a useful clinical tool for diagnostic and/or treatment decisions.

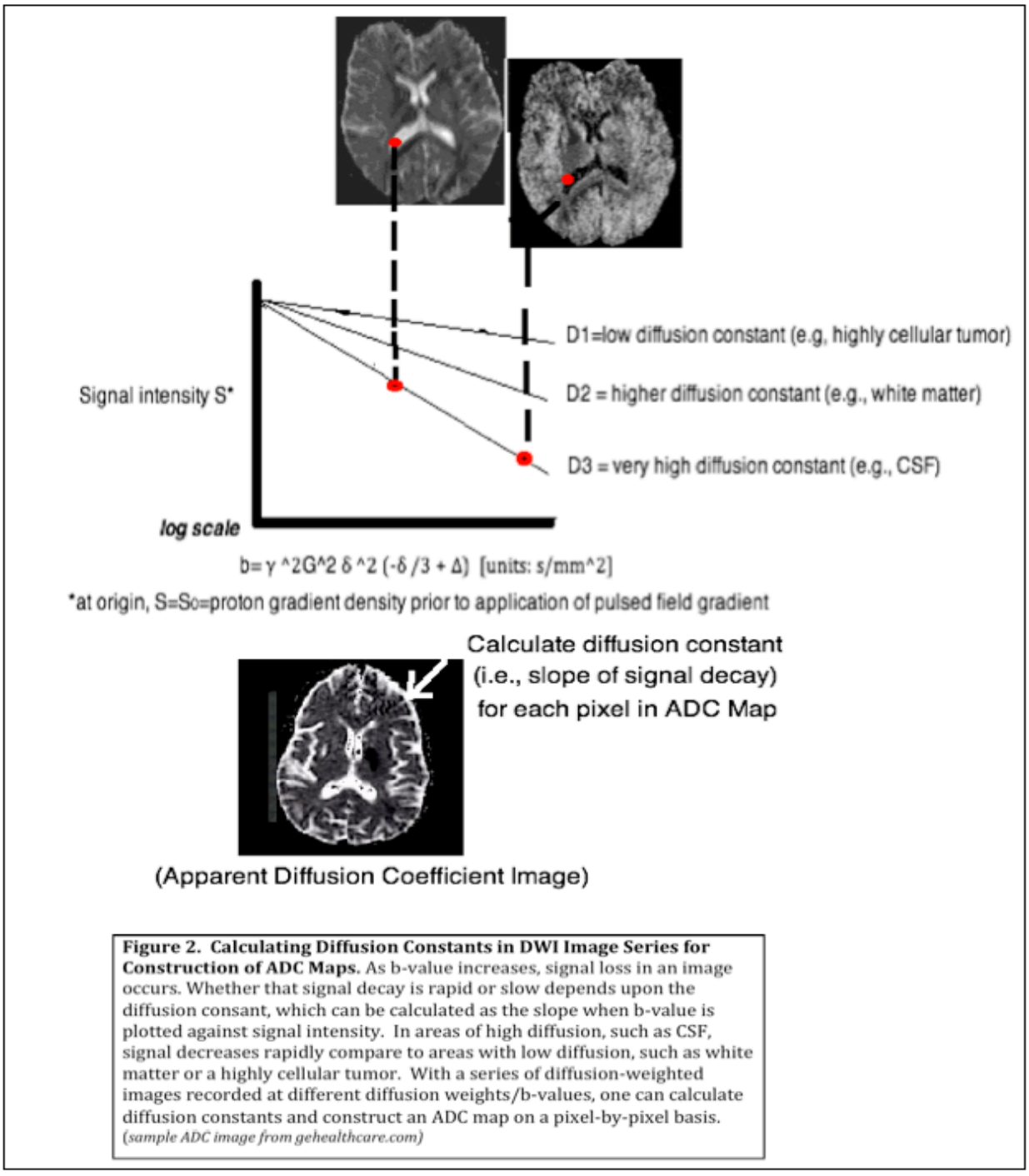

Figure 2. Calculating Diffusion Constants in DWI Image Series for Construction of ADC Maps. As b-value increases, signal loss in an image occurs. Whether that signal decay is rapid or slow depends upon the diffusion consant, which can be calculated as the slope when b-value is plotted against signal intensity. In areas of high diffusion, such as CSF, signal decreases rapidly compare to areas with low diffusion, such as white matter or a highly cellular tumor. With a series of diffusion-weighted images recorded at different diffusion weights/b-values, one can calculate diffusion constants and construct an ADC map on a pixel-by-pixel basis. *(sample ADC image from gehealthcare.com)*

Clinical Applications of Diffusion-Weighted Imaging

In the clinical setting, DWI has proven most useful in distinguishing between cytotoxic and vasogenic edema in cerebral ischemia. (39, 40) In vasogenic edema, tight endothelial junctions comprising the blood-brain-barrier (BBB) are disrupted, resulting in variable signal intensity on DWI and higher ADC due to spread of protein and fluids into the extracellular space. (41) Conversely, restricted diffusion with DWI

hyperintensity and low ADC is observed in cytotoxic edema, reflecting a loss of extracellular fluid with commensurate swelling of intracellular compartments due to cellular retention of sodium and water from ATP depletion and consequent failure of the Na+/K + ATPase. (42,43) Cytotoxic edema is most characteristic of early acute ischemia, with changes in ADC occurring with minutes after onset, but can also be seen with various intoxications, encephalopathies, hypoglycemia, status epilepticus, or any other non-ischemic cause of deranged cellular metabolism. (44) Conversely, T2-weighted images will remain normal for several hours, eventually displaying an increase in intensity due to vasogenic edema. (45) ADC values in acute stroke reach their nadir by 24 hours and persist for 1-2 weeks, and although “cytotoxic edema” is repeatedly attributed as the explanation for persistent changes on DWI, (46) several researchers have suggested there are likely to be other mechanisms underlying ADC change that have not yet been elucidated. (47) Nevertheless, DWI has proven very sensitive (although some lacunar infarcts may not be detected) and reasonably specific in early detection of acute ischemic stroke during the crucial ‘window of opportunity’ for therapy. (48)

In recent years, research into clinical applications of DWI has greatly expanded in an attempt to better characterize neurologic disorders other than acute stroke. (49) For example, movement disorders including Parkinson’s disease, progressive supranuclear palsy, and multiple system atrophy (50,51) have been studied with a ROI-based approach that readily differentiated some of these conditions on the basis of DWI findings. Diffusion MRI has also been employed in studying features of Alzheimer’s Disease (AD) and non AD-type dementias, (52)

early diagnosis of Creutzfeld-Jakob disease, (53) multiple sclerosis, (54) herpes encephalitis, (55) and epilepsy (including status epilepticus, interictal phases, and single seizures). (56) In addition, DWI has been used to differentiate arachnoid and epidermoid cyst (57) and subtypes of brain abscesses, including differentiation of pyogenic abscess from necrotic tumor. (58) This list is far from comprehensive, as an explosion of clinical literature utilizing this technique has occurred in a relatively short period of time, reflecting the tremendous potential of diffusion imaging for use in the clinical setting.

The literature concerning DWI in diagnostic evaluation of patients with brain tumors has increased particularly rapidly; several recent studies have attempted to correlate ADC with cellularity or grade of various tumors, assess infiltration into peritumoral edema, or differentiate among tumors that can otherwise appear similar using conventional MR techniques (e.g. PCNSL, glioblastoma multiforme, anaplastic astrocytoma, metastases). (59) Many early studies, however, were not encouraging; for example, a study aimed at distinguishing between tumor tissue and peritumoral edema in gliomas found no ability to differentiate on the basis of absolute ADC values or ADC ratios. (60) Another study found that ADC was helpful in grading of malignant brain tumors in a sample of 33 low-grade (23 astrocytomas, 10 oligodendogliomas) and 40 high-grade (25 metastases, 15 high-grade astrocytomas) neoplasms, but was unhelpful in differentiation among them. (61) In a 2001 study examining 56 patients with the three most common types of intracranial neoplasms (gliomas, metastases, and meningiomas), too much variation existed within each group to reliably differentiate among them on the basis of either DWI or ADC maps.

(62) Furthermore, the authors were unable to successfully use either DWI or ADC to assess tumor infiltration or differentiate infiltration from perifocal edema, which contradicted a previous report. (63) Another 2001 study found considerable overlap in ADC values and could not separate tumor from surrounding edema in a small sample of patients with high-grade cerebral glioma. (64) A third 2001 study found no advantage of DWI in evaluating tumor extension in a sample of patients with gliomas, metastases, meningioma, and abscess. (65)

This led a member of the editorial board of the neuroradiology journal in which several of the above articles were published to state in 2001 that “the bloom [is] off the rose” with respect to the use of DWI in evaluation of brain tumors: “There is a natural history for new diagnostic tests. The initial results are amazing, the praise overwhelming. The test is viewed as having almost magical qualities. After a while, reality sets in. The initial enthusiasm wanes as experience accumulates. This is where we are now with diffusion-weighted imaging.” (66) Yet, the author concluded that DWI was nevertheless a potentially valuable tool, particularly when studies utilized a quantitative analysis of specified ADC regions of interest, as a more sensitive way of revealing significant abnormalities that may not be readily apparent simply by looking at a diffusion-weighted image or ADC map.

A small number of studies have begun to characterize DWI findings in patients with PCNSL, (67,68) attempt to differentiate between PCNSL and other tumors on the basis of DWI, (69,70,71,72,73,74) and even utilize ADC as a predictor of clinical outcome and response to therapy. (75) Yet, the body of literature available for comparison of findings in PCSNL remains relatively small, as does the sample

size in individual studies. Additionally, studies utilizing DWI in the characterization of PCSNL continue to appear with findings that contradict prior reports; as recent as 2009, Server et al. found no significant difference between malignant gliomas and PCSNL on the basis of DWI. (76) Is the “bloom off the rose” in the case of diffusion-weighted imaging in PCNSL, or will ADC be established in time as a surrogate marker of cellularity to characterize and differentiate among tumors, and perhaps even predict therapeutic response? Given the need for additional clarity in the relatively meager and sometimes conflicting literature, and as the incidence of PCNSL continues to rise in the population, we conducted a retrospective study utilizing a comprehensive neuroimaging protocol including DWI and quantitative ADC region of interest analysis to better characterize the MRI appearance of this disease.

Statement of Purpose:

The purpose of this investigation was to identify and characterize the earliest DW-MRI findings in patients with PCNSL prior to corticosteroid use or other therapy. Quantitative region of interest analysis was performed using parametric ADC maps. ADC values derived from this study were then compared to measurements from other studies via a comprehensive review of prior investigations utilizing DWI in the evaluation of PCNSL. The hypothesis was that restricted diffusion is a reliable marker of increased tumor cellularity in PCNSL, and that ADC values may be useful to differentiate PCNSL from other intracranial lesions.

Methods

Disclosure statement: All MRI protocols were performed by clinicians at Yale-New Haven Hospital and Massachusetts General Hospital. Study was conceived and identification of patient cohort was performed by J.M.B., S.B., E.H., and F.H.H. Quantitative DW-MRI region of interest analysis and selection, abstraction, and review of prior literature for comparison with the measurements derived in this thesis was performed by J.W.G. with R.K.F. as primary advisor.

This project was approved by the Human Investigation Committee at Yale University School of Medicine and the Internal Review Board at the Massachusetts General Hospital.

Subjects

Three databases were accessed to gather subjects: the Connecticut Cancer Registry, the Yale School of Medicine (New Haven, CT) Brain Tumor Center database, and the Massachusetts General Hospital (Boston, MA) Brain Tumor Center database. The dates evaluated were between January 1982 and July 2007 for the Connecticut and Yale databases, and between January 2000 and June 2007 for the MGH database. Patients with PCNSL were included only if they had a histopathologically confirmed diagnosis. Exclusion criteria included congenital or acquired immunodeficiency (e.g., HIV), lymphoma without cerebral involvement (e.g., primary intraocular lymphoma), or patients where insufficient clinical information was available to ascertain appropriateness for inclusion (e.g., missing histopathology report or imaging data at diagnosis).

137 immunocompetent patients with PCNSL were initially identified, including 45 cases from Yale and 95 cases from MGH. Of these, 56 cases were excluded due to insufficient data or lack of access to imaging performed at the time of initial diagnosis. In addition, nine cases were primary intraocular lymphoma without CNS

spread, leaving a total of 72 cases meeting entry criteria. Of these, sixteen cases with DWI data and ADC maps available in PACS for region of interest analysis were identified. Four were excluded due to insufficient data, leaving a final cohort of 12 cases for quantitative DW-MRI analysis. The study cohort includes 9 men and 3 women with a median age of 48.5 years (range 14-73), including one pediatric case aged 14 at time of diagnosis.

MR Imaging

This study was retrospective in nature, so MRI protocols and timing are not standardized among patients. A 1.5T MR Imaging unit was used at both Yale-New Haven Hospital and MGH. T1-weighted spin-echo images were obtained in axial, coronal, and sagittal planes with the following parameters: repetition time [TR]=600 ms; echo time [TE]=20 ms; number of excitations=1, and long-TR dual-echo axial sequences (2500/30.9/1). Other imaging parameters include: field of view=21 cm, 256x192 matrix slice thickness 5 mm with spacing of 0-2 mm. T1-weighted axial images were obtained before and after intravenous administration of gadopentate dimeglumine contrast medium (0.1 mmol/kg). ADC maps were generated based on diffusion-weighted echo planar sequences. Six high b-value images (1000 mm^2/s) and one low b-value images (3 mm^2/s) were acquired for each of 23 axial slices. The following parameters were used: TR=10 s, TE=104 ms, diffusion encoding gradients=45 ms, 128x128 matrix, field of view, 24.5 mm slice thickness, 1mm spacing, one signal average.

Imaging Analysis

Postprocessing of apparent diffusion coefficient (ADC) maps and values occurred on a Siemens workstation (Siemens Medical Solutions, USA). DWI images and ADC maps were aligned with contrast-enhanced T1-weighted and FLAIR images corresponding to the same section level. Patients were retrieved from PACS using a combination of date and medical record number, and all images retrieved were rendered anonymous and free of any patient identifiers. ROIs were drawn from the solid enhancing region of tumor, peritumoral edema, and contralateral normal-appearing white matter (**Figure 1)** using a circular pixel lens tool available in the workstation**.** All ROIs drawn were approved by a neuroradiologist blinded to all information other than diagnosis (R.K.F.). ROI areas ranged between 0.47-0.78 cm^2 and were drawn to avoid necrotic or hemorrhagic areas. Values for ADC mean, minimum, and standard deviation were calculated. Ratios (ADC of tumor focus to ADC of peritumoral region; ADC of tumor focus to ADC of contralateral normal white matter) were also calculated. Inter-group variance in mean ADC values between ROI groups was assessed using one-way Analysis of Variance (ANOVA). All ADC values are reported as 100 x 10^-6 mm^2/s. Pairwise post-hoc comparison of mean ADC values between groups was performed using Tukey's HSD test at the $p<0.01$ level of significance.

Literature selection

Prior studies utilizing DWI in the study of PCNSL were chosen by searching MEDLINE, Web of Science, and Google Scholar for articles listed between 1992

(when DWI was first used in the early diagnosis of cerebral ischemia) and 2010. Relevant search terms were used, including any combination of “diffusion-weighted imaging,” “diffusion imaging,” “DWI,” “DW-MRI,” or “diffusion MR imaging” with “primary CNS lymphoma,” “central nervous system lymphoma,” “primary lymphoma of the central nervous system,” “brain lymphomas,” “cerebral lymphoma,” or “PCNSL”. After scanning titles and abstracts, relevant full articles were reviewed to select those reporting original research using quantitative ADC/DWI measurements. In addition to these measurements, the following information was retrieved for each study: authors, year of publication, number of cases, average age of patients, stratification of patient groups, and methods of ROI drawing and ADC calculation.

Figure 1: Apparent diffusion coefficient (ADC) map (a) and axial gadolinium contrast-enhanced T1-weighted MR image (b) at same level in case of primary CNS lymphoma. ROIs are placed centrally in the core of the lesion, in the adjacent peritumoral edema, and in contralateral normal white matter.

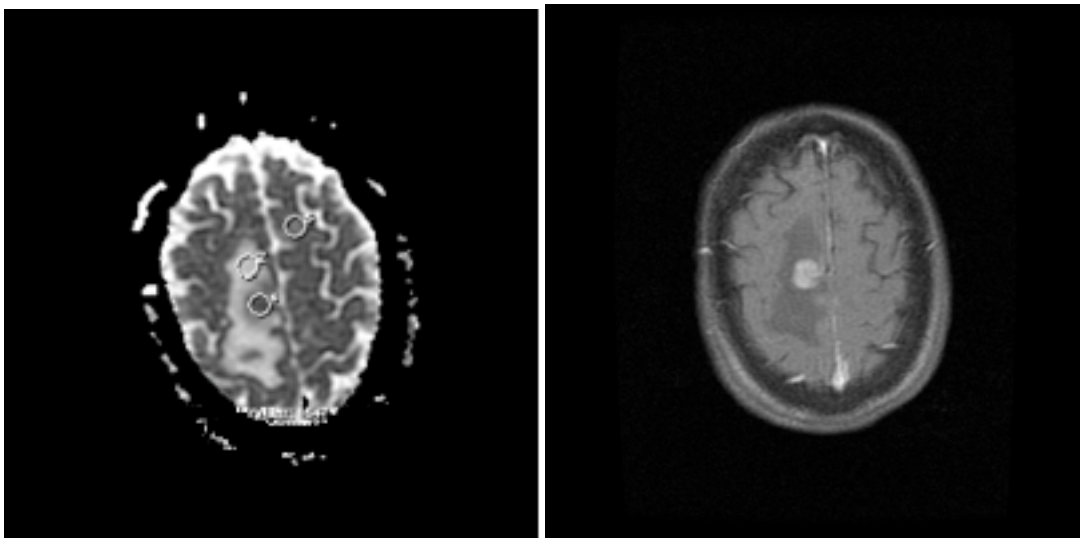

(a) **(b)**

Results

ROI analysis was performed for cases with DWI and ADC maps available (n=12), an example of which is illustrated in **Figure 2.** The mean ADC and range of the enhancing portion of PCNSL lesions was 888 +/- 137 $x10^{-6}$ and 609-1065 x10^-6 mm^2/s, respectively. The minimum ADC and range of the enhancing portion of lesion was 704 +/-185 $x10^{-6}$ and 326-947 $x10^{-6}$ mm^2/s, respectively. The mean ADC and range of the peritumoral region was 1429 +/- 272 $x10^{-6}$ and 1162-1934 $x10^{-6}$ mm^2/s, while the mean ADC and range of contralateral normal-appearing white matter was 878 +/- 146 $x10^{-6}$ and 578-1083 $x10^{-6}$ mm^2/s, respectively. The ADC ratio of the enhancing portion of the lesion to surrounding perifocal edema was 0.64 +/-0.13, while the ratio of the enhancing portion of lesion to contralateral normal-appearing white matter was 1.12 +/-0.07.

One-way Analysis of Variance (ANOVA) revealed significant inter-group variance between the mean ADC of lymphomas, peritumoral regions, and contralateral normal white matter ($F(2,33)=31.438$, $p<0.001$). Tukey post-hoc comparison of the three groups indicate that the mean ADC of the peritumoral lesion is significantly different from the mean ADC of the lesion and normal white matter. However, differences between mean ADC of lesion and normal white matter were not statistically significant at $p<0.01$.

Our literature search for prior studies of DWI in PCNSL revealed 13 articles that met eligibility criteria for comparison, describing a total of 133 separate patients with lymphomas for which DWI/ADC quantitative measurements were recorded

(Table 1). Ten out of thirteen reported ADC values of lymphoma lesions as means, four studies reported ADC minimums, and two studies reported ADC medians. One study provided data on 25th percentile ADC values and another reported ADC maximums. Two out of thirteen did not provide complete information regarding standard deviation of reported values, and three out of thirteen did not provide a range of values. In two studies, range could only be approximated based on boxplot data. Two out of thirteen reported ADC measurements from perilesional edema or contralateral normal white matter; in one additional study, the mean ADC value for normal white matter was approximated from the reported ADC ratio of lesion to contralateral normal white matter. This ratio was reported in five out of thirteen studies. However, only one study prior to ours reported a ratio of lesion to surrounding peritumoral edema. Most studies reported data from immunocompetent patients or did not specify patient immune status; however, one study (Camacho et al.) was strictly limited to AIDS patients, another (Kitis et al.) stratified ADC values into immunocompetent and immunocompromised patient groups, and a third (Zacharia et al.) included both immunocompetent and immunocompromised individuals but stratified ADC reporting based on pattern of enhancement rather than immune status. Additional details of individual studies are addressed in the Discussion.

Table 1: Comparison of Diffusion-Weighted Imaging Findings in PCNSL.

All ADC values reported (x10^-6 mm^2/s).	*N*	ADC_{lesion}	Range	$ADC_{perilesion}$	ADC_{normal}	Ratio ADC lesion/normal	Ratio ADC lesion/perilesion
Our Data	12	888+/-137 (mean)	609-1065	1429+/-272 (mean)	878+/-146 (mean)	1.02+/-0.07	0.64+/-0.13
Guo et al., 2002	11	870+/-270 (mean)	n/a	n/a	750 +/- 40 (mean)	1.15+/-0.33	n/a
Camacho et al., 2003 (*AIDS* patients)	4	930(SD n/a) (mean)	670-1200	n/a	n/a	1.14+/-0.25	n/a
Kitis et al., 2005 *Immunocompetent* *Immunocompromised*	8 6 2	540+/-100 (min) 550+/-120 (min) n/a	350-670 n/a n/a	n/a	n/a	n/a	n/a
Yamasaki et al., 2005	8	725+/-192 (mean)	504-1067	n/a	n/a	n/a	n/a
Calli et al., 2006	8	510 +/- 90 (min)	~400-650	n/a	n/a	n/a	n/a
Reiche et al., 2007	4	757 (median)	602-860	1567 (median)	n/a	n/a	n/a
Al-Okaili et al., 2007	12	860+/- 220 (mean) 990 (median)	370-1100	n/a	n/a	n/a	n/a
Toh et al., 2008	10	630+/-155 (mean)	371-806	n/a	752 +/-86 (mean)	0.83+/-0.14	n/a
Akter et al., 2008 *DWI-Hyperintense* *Partial Hyperintense* *Isointense*	16 (9) (4) (3)	780+/-170 690+/-140 840+/-110 960+-210 (mean)	n/a	n/a	n/a	n/a	n/a
Zacharia et al., 2008 *Homo/Heterogeneous* *Ring enhancing - (Lesion Periphery)*	20 (15) (5)	 650+/- 43 720+/-41	 570-720 650-800	n/a	n/a	n/a	n/a

- (Lesion Center) *Post-Treatment*	 (7)	1140+/-20 n/a (mean)	1060-1210 860-1140				
Horger et al. 2009	9	710+/-130 (mean)	~500-900	n/a	n/a	0.93+/-0.19	n/a
Server et al., 2009	5	732+/-170 (mean) 648+/-155 (min)	n/a	1.59+/-0.27 (mean) 1.49+/-0.24 (min)	~711 (mean, approx.)	1.03+/-0.24 (mean) 1.03+/-0.26 (min)	0.46+/-0.08 (mean) 0.43+/-0.08 (min)
Barajas et al., 2010 *Response Groups* *- Primary Refractory* *- Clinical Response*	18 (7) (11)	830(SD n/a) (mean) 377(SD n/a) (min) 757+/-96 (mean) 244+/-84 (min) 876 +/-74 (mean) 462+/-98 (min)	636-1016 (mean) 167-614 (min)	n/a	n/a	n/a	n/a

Figure 2: Typical DWI findings in PCNSL. Diffusion-weighted imaging (A) shows hyperintensity corresponding to a right occipital mass, while ADC map (B) shows low signal consistent with restricted diffusion. Gadolinium contrast-enhanced T1-weighted imaging shows strong homogeneous enhancement in the mass (C), which can be seen on FLAIR (D) to invade the splenium of corpus callosum and right lateral ventricle.

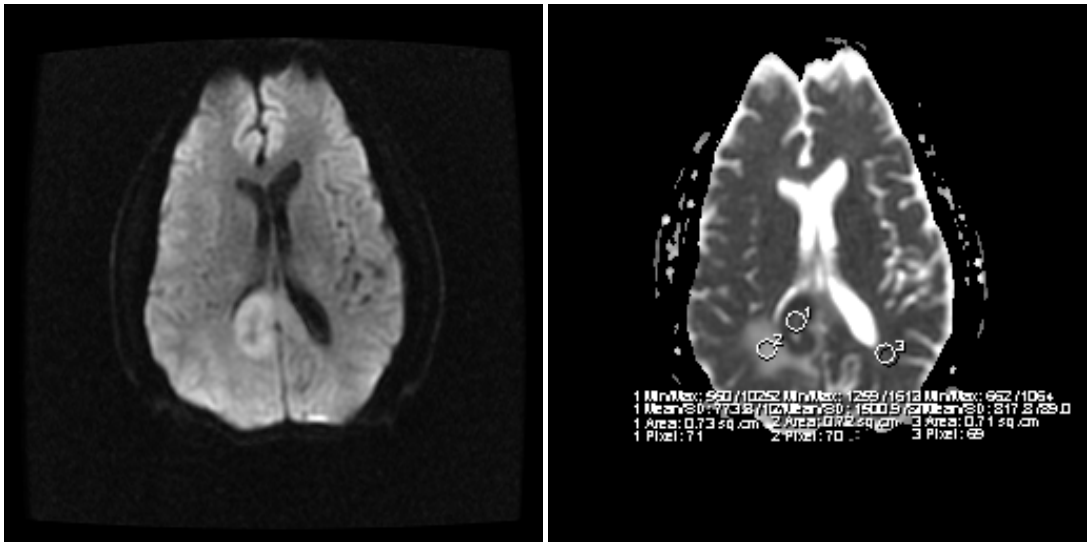

A **B**

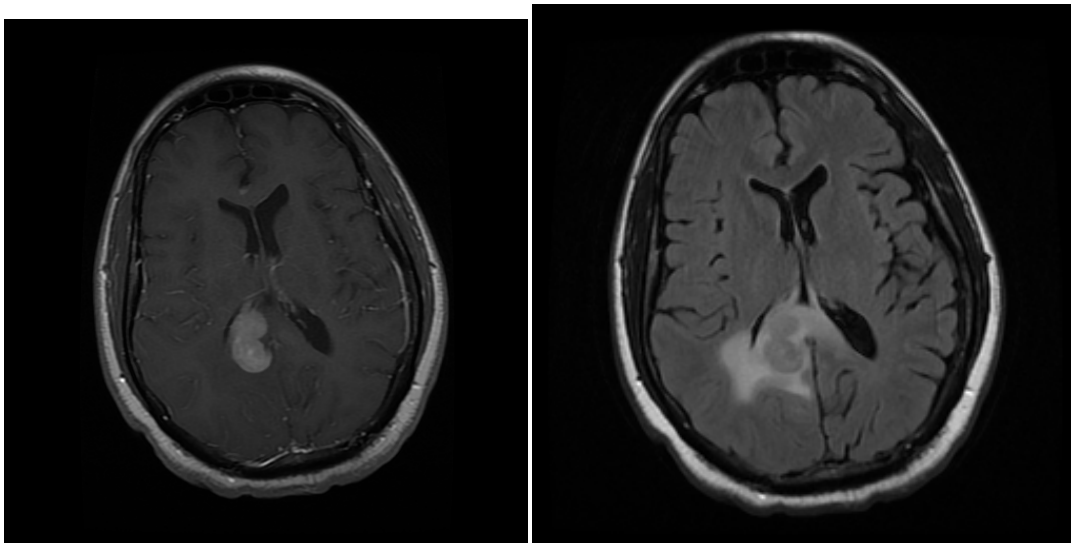

C **D**

Discussion

A small number of studies have attempted to characterize DWI findings in PCNSL, (65-68, 77) differentiate between PCNSL and similarly appearing tumors, (69-74) or predict response to therapy and clinical outcome. (75) DWI is thought to provide information about tumor cellularity or grade because water diffusion correlates highly with the ratio of extracellular to intracellular space, (33,41) with greater diffusion expected in an extracellular medium. (37) A highly cellular tumor such as PCNSL serves as a significant barrier to water diffusion by decreasing the volume and increasing the tortuosity of the extracellular space, which is (in theory) reflected as a relative decrease in ADC value and increased signal on DWI compared to less cellular tumors.

Although several groups have provided data in support of restricted diffusion as a consistent finding on DWI in PCNSL, to date there has not been a comprehensive review of quantitative methods and measurements among investigators. We presented the ADC values derived in our study with a summary of findings from prior work in Table 1**.** The earliest quantitative study using ADC values in PCNSL was a 2002 retrospective series of 19 brain lymphomas in 11 patients by Guo et al., which used ADC ratios of tumor to normal-appearing regions in a small cohort of patients with either lymphoma or astrocytoma. (69) Sixteen of nineteen lesions appeared hyperintense on DWI and iso- to mildly hypointense on ADC signal; additionally, an inverse correlation between diffusion and cellularity was reported based on calculation of nuclear-to-cytoplasmic (N/C) ratios in histologic samples. However, the correlation between ADC values and N/C ratios was

relatively modest (r=-0.46). A later study confirmed an inverse correlation between mean ADC and cellular density of similar magnitude (r=-0.54). (75) This suggests that factors other than tumor cellularity are at play in determining ADC values, which may include degenerative changes such as hemorrhage or abscess and local effects due to expression patterns of hydrophilic components of the extracellular matrix. (78) PCNSL in immunocompetent patients is typically a non-necrotic, homogeneous-appearing tumor lacking these confounding degenerative changes; thus, it is believed that DWI represents a potentially useful and specific diagnostic tool for this disease.

In a similar series of 16 patients with PCNSL, thirteen (80%) were hyperintense or partially hyperintense on DWI, which corresponded to lower overall mean ADC values than isointense lesions; however, significant overlap existed between all three groups. (79) Zacharia et al. studied 20 patients comprising both immunocompetent and immunocompromised as well as pre- and post- treatment cases, finding areas of restricted diffusion in 90% (18/20) of pretreatment scans. (67) The ADC range was higher with significant variability in both post-treatment and immunocompromised individuals, presumably reflecting low cellularity as a consequence of increased necrosis and partial volume effect due to decreased lesion size. Another issue was highlighted in Reiche et al.'s DWI study of four PCNSL cases, one of which displayed an absent enhancement pattern that delayed time to diagnosis and biopsy. (68) This pattern of enhancement is a rare but known (80) presentation of PCNSL and underscores the potential of DWI—which showed

lesions in this case to be hyperintense with low ADC suggestive of a hypercellular neoplasm—to provide clues in difficult diagnostic situations.

A number of investigators have attempted to use DWI to distinguish PCNSL from other lesions that appear similar on conventional MRI (e.g. glioblastoma multiforme, anaplastic astrocytoma, some highly cellular metastases). One such study used minimum ADC values to differentiate low-grade gliomas from high-grade gliomas, metastases, and lymphomas, observing consistently low ADC values for the latter; however, this difference did not achieve statistical significance and the range of lymphoma ADC values overlapped with those of high-grade gliomas. (81) Server et al. also found no significant difference between malignant gliomas and PCSNL with DWI. (76) A third group found no difference on the basis of either mean ADC of enhancing tumor or ADC ratio of tumor to uninvolved white matter between lymphoma and glioblastoma in a study restricted to invasion of the corpus callosum. (72) However, echoing an earlier report by Guo et al., they did find a significant difference on the basis of ADC values between lymphomas and astrocytomas. In contrast to the prior studies, a report by Calli et al found a significant difference between lymphomas and both GBMs and AAs on the basis of minimum ADC values. (73) Similarly, Toh et al. and Yamasaki et al. found a significant difference between PCNSL and GBM based on ADCs. (70-71) However, there was considerable overlap in the range of values between groups in all three of these studies. This conflicting evidence highlights the lack of clarity in the literature and the importance of interpreting potentially variable ADCs in the context of a full clinical and MR imaging evaluation.

DW-MRI has also been used to evaluate select populations in which the differential diagnosis of brain masses can be particularly challenging, such as patients with AIDS. In these individuals, toxoplasmosis and PCNSL are the two most common etiologies. The characteristic rim-enhancement and profound vasogenic edema of infectious abscess is often difficult to distinguish from tumor in immunocompromised hosts. Camacho et al. used ADC values to differentiate PCNSL from toxoplasmosis in patients with AIDS, and although there was a statistically significant difference between the two groups, there was again considerable overlap in the range of ADC values. (82)

Overall, there is a demonstrated trend of either negative results or reports of statistical significance belied by significant overlap between ADC values in the literature regarding use of DWI in differential diagnosis of PCNSL. This is consistent with several studies that have reported negative results attempting to use DWI or ADC maps to differentiate between various tumors not including PCNSL, or between tumor tissue and surrounding edema. (4,60-64) The range of values that we derived with a patient population and methods similar to prior reports also overlap significantly with reported range of ADCs for other tumors. Even for studies strictly limited to characterization of PCNSL, there is substantial variation in the range of ADC values reported. Among all studies, values ranged from 371-1200 x 10^{-6} mm^2/s for the solid enhancing portion of a PCNSL lesion, and mean values ranged from 650 – 930 x 10^{-6} mm^2/s **(Table 1)**. There is also a lack of consensus regarding which DWI metrics are most informative—investigators have reported ADC values in terms of means, medians, minimums, 25th percentiles, ratios, values for

homogeneously/heterogeneously enhancing vs. ring-enhancing portions of lesions, values for individual lesions vs. averages of regions from several lesions, and so forth. While there is intrinsic appeal to a DWI region of interest method where one can choose locations based on an *a priori* hypothesis about the relationship between tumor cellularity and ADC, there are other complex underlying pathological processes that influence the value obtained, thus rendering conclusions drawn from these widely varying and overlapping ADC ranges tenuous. Future studies comparing groups of tumors should establish firm “threshold” levels above or below which lesions can be differentiated with near-100% accuracy, rather than report a statistically significant difference between two overlapping ranges of values that are of little clinical benefit out of context.

In addition to variance in how investigators choose to report ADC values and heterogeneity of PCNSL appearance and presentation, several other limitations of our study and the studies summarized in Table 1 account for the discrepant evidence in the literature. Many conclusions are based on a very small sample size (as few as 4 lesions), or with significant error in values reported (in the Guo et al. series, the standard deviation of the mean ADC for PCNSL lesions was 31% of the estimate itself). Variability is also introduced by using less than six *b* values in generation of an ADC map, and many of these studies used such a technique (although studies have shown that the error used by this method is small). (83) The sampling method is also a significant potential source of confounding. This includes error inherent to the subjective process of manually positioning regions relative to affected anatomical structures, difference of opinion among investigators regarding

whether areas of degeneration or necrosis or vascular territories should be included or excluded from regions of interest, (84) “normal-appearing” tissue on MR imaging actually representing underlying pathology and inappropriately being used as a tissue reference, and errors inherent to faulty software co-registration of images. Owing to the retrospective nature of these studies, some relevant images and clinical information or cases may have been missed. Patients exposed to corticosteroids or other conditions that could have altered the appearance of images used in analysis may have also been included inappropriately. Large-scale prospective studies in the future with strictly defined criteria for pre-treatment ADC determination should serve to address some of these issues.

One other issue of note highlighted by our data is the lack of difference between mean ADC of the enhancing portion of PCNSL lesions and ADC of contralateral normal white matter. Less than half of prior studies measuring ADC values for PCNSL reported ratios normalized against normal white matter **(Table 1)**. Although our absolute value for ADC of contralateral normal tissue is the highest among the studies that have reported these values, our ratio of ADC (lesion/normal) is in line with prior estimates, which have ranged from 0.83 to 1.15 with a standard deviation between 0.07 and 0.33 **(Table 1)**. That these estimates typically include a possible ratio of 1 suggests little difference between the ADC of an enhancing PCNSL lesion and uninvolved normal white matter, which is surprising given the inverse relationship between cellularity and diffusion emphasized in the literature and the dramatically restricted diffusion relative to normal tissue one might expect in a highly cellular environment. This suggests that ADC measurements are not as

highly correlated with cellularity as imagined, and subject to other biophysical forces that remain poorly understood. One possibility may be related to the pathologic and histologic features of PCNSL, which are remarkable in that neoplastic cells tend to congregate in sheets along vascular channels. (85) It has been theorized that the mechanism of PCNSL spread is through enlarged perivascular (Virchow-Robin) spaces with infiltration of vessel walls. (86) This phenomenon may also predispose to partial volume effects with entrapped interstitial fluid in perivascular regions or vasogenic edema within lesions that could affect ADC values obtained. Additionally, while the absolute ADC value may not be helpful in delineating between normal white matter and PCNSL lesions, the ratio of lesion to perifocal edema highlighted a consistent and significant difference in our series. Our values are consistent with the one other study that reported this ratio **(Table 1)**. Further research will be necessary to determine if the values we obtained for this ratio are reasonably specific for PCNSL.

Where does the future lie with regard to use of DWI in clinical evaluation of PCNSL? Current research is aimed at investigating its use in predicting clinical response and therapeutic outcome. In the past, DWI has been used to distinguish tumor recurrence from radiation-induced necrosis (87-88) or postoperative changes (89) and detect early response to therapy in brain tumors, (90-91) although conflicting studies have shown both increased (92) and decreased (93) ADC in response to treatment. Functional diffusion maps, in which voxel-by-voxel changes in ADC measurements are tracked through serial DWI, have also been shown to track tumor growth in gliomatosis cerebri (94) and predict treatment response in a

variety of tumors (not including PCNSL). (95-96) Barajas et al. tested the hypothesis that tumor cellular density in PCNSL as reflected by pre-treatment ADC values within contrast-enhancing regions of tumor could be used to predict clinical outcome. (75) Patients with 25^{th} percentile ADC values <692 and minimum ADC values <384 x 10^{-6} mm^2/s predicted disease refractoriness as measured by shorter progression-free and overall survival, while those above those thresholds had a reduction in post-treatment ADC values and improved survival. (11) The authors state that the reduction in ADC values in the "high ADC" group might be due to reduced extracellular diffusion secondary to cellular swelling as a consequence of responsiveness to chemotherapy. However, the distance between treatment initiation and post-treatment imaging (up to several months) argues against this hypothesis. Regardless, the evidence that ADC is able to serve as a surrogate marker for therapeutic response is encouraging, and interest in post-treatment surveillance imaging biomarkers should remain high as chemotherapeutic and radiation therapy options advance and improve outcomes.

The future of PCNSL imaging research lies also in the use of more sophisticated techniques. For example, diffusion is frequently anisotropic in the brain while "basic" DWI only measures diffusion speed along one direction. By varying the orientation of the MRI diffusion gradient along orthogonal directional axes, differences in diffusion and image contrast can be observed. (97) This technique, known as diffusion tensor imaging (DTI), is increasingly being used in the evaluation and differential diagnosis of PCNSL with promising initial findings; for example, fractional anisotropy (FA, an index of diffusion anisotropy that reflects the

microarchitecture of CNS white matter fibers) was significantly lower in PCNSL vs. GBM. (71, 98) Given that the directionality data in DTI could theoretically be applied to provide structural information regarding unique features of localization/infiltration of PCNSL lesions relative to white matter tracts, and that FA has been correlated strongly with cellularity, (99) it is likely that the body of literature studying not only DWI but also DTI in the evaluation of PCNSL will continue to expand.

Taken together, our results support restricted diffusion as a consistent DWI finding in PCNSL, particularly as compared to peritumoral edema. This view is in accord with prior studies that have demonstrated an inverse correlation between ADC and cellularity of lesions. However, the reported strength of this relationship is modest, presumably due to other factors affecting ADC measurements that, in addition to methodological differences and other limitations of prior studies, account for the variance of values reported in the literature. There is currently insufficient evidence to advocate the use of ADC values as a definitive basis for differential diagnosis of intraaxial brain masses, as the ranges of ADC values reported for lymphoma frequently overlap with those of other tumors. However, in difficult diagnostic situations where clinical information and conventional MR imaging data is insufficient to render a diagnosis, use of DW-MRI may be helpful as an adjunct to point the clinician in the right direction, as in the example of a rare non-enhancing lymphoma lesion displaying restricted diffusion with a low ADC. Additionally, imaging strategies that incorporate multiple techniques may represent a path forward; for example, a recent study combined conventional MR imaging, perfusion MR imaging, and proton MR spectroscopy to differentiate high-grade neoplasms and lymphoma

from low-grade neoplasms and noncancerous lesions with an accuracy and sensitivity of 85% and 84%. (74) Ultimately, there remains no substitute for clinical judgment. Caution must be urged against overreliance upon quantitative measurements when arriving at a final diagnosis, and such data should always be interpreted in the context of the patient's full clinical presentation.

References

[1] Hochberg, F., Baehring, J., & Hochberg, E. (2007). Primary CNS lymphoma. *Nature Clinical Practice Neurology , 3* (1): 24-35.

[2] Gerstner, R., & Batchelor, T. (2010). Primary central nervous system lymphoma. *Arch Neurol, 67* (3): 291-7.

[3] Central Brain Tumor Registry of the United States (2010). Statistical Report: Primary Brain Tumors in the United States 2004-2006. [http://www.cbtrus.org/reports]

[4] Hochberg, F., & Miller, D. (1988). Primary central nervous system lymphoma. *Journal of Neurosurgery, 68* (6): 835-53.

[5] Diamond, C., Taylor, T.H., Im, T., Miradi, M., Wallace, M., & Anton-Culver, H. (2006). Highly active antiretroviral therapy is associated with improved survival among patients with AIDS-related primary central nervous system non-Hodgkin's lymphoma. *Curr HIV Res, 4*: 375-8.

[6] Olson, J., Janney, C., Rao, R., Cerhan, J., Kurtin, P., Schiff, D., et al. (2002). The continuing increase in the incidence of primary central nervous system non-Hodgkin lymphoma: a surveillance, epidemiology, and end results analysis. *Cancer, 95* (7): 1504-10.

[7]Bataille, B., Delwail, V., Menet, E., et al. (2000). Primary intracerebral malignant lymphoma: report of 248 cases. *Journal of Neurosurgery, 92* (2): 261-66.

[8] Salih, B.S., Saeed, A.B., Alzahrani, M., Al Qahtani, M., Haider, A., Palker, V. (2009). Primary CNS lymphoma presenting as fever of unknown origin. *J Neurooncol, 93* (3): 401-4.

[9] Layden, B.T., Dubner, S., Toft, D.J., Kopp, P., Grimm, S., & Molitch, M.E. (2009). Primary CNS lymphoma with bilateral symmetric hypothalamic lesions presenting with panhypopituitarism and diabetes insipidus. *Pituitary* [Epub ahead of print.]

[10] Intraocular-central nervous system lymphoma: clinical features, diagnosis, and outcomes (2000). *Ocul Immunol Inflamm, 8* (4): 243-50.

[11]Brecher, K., Hochberg, F.H., Louis, D.N., de la Monte, S., & Risking, P. (1998). Case report of unusual leukoencephalopathy preceding primary CNS lymphoma. *J Neurol Neurosurg Psychiatr, 65* (6): 917-20.

[12]Yang, J-H, & Wu, S-L. (2007). Multiple sclerosis preceding CNS lymphoma: a case report. *Acta Neurol Taiwan*, *16* (2): 92-7.

[13]Burgetova, A., Seidl, Z., Vaneckova, M., & Jakoubkova, M. (2008). Concurrent occurrence of multiple sclerosis and primary CNS lymphoma: a case report. *Neuro Endocrinol Lett*, *29* (6): 867-70.

[14]Alderson, L., Fetell, M.R., Sisti, M., Hochberg, F., Cohen, M., Louis, D.N. (1996). Sentinel lesions of primary CNS lymphoma. *J Neurol Neurosurg Psychiatr, 60* (1): 102-5.

[15]Ng, S., Butzkueven, H., Kalnins, R., & Rowe, C. (2007). Prolonged interval between sentinel pseudotumoral demyelination and development of primary CNS lymphoma. *J Clin Neurosci, 14* (11): 1126-9.

[16] Cha, S. (2009). Neuroimaging in neuro-oncology. *Neurotherapeutics, 6* (3): 465-77.

[17] Ricci, P.E. (1999). Imaging of adult brain tumors. *Neuroimaging Clin N Am, 9*: 651-69.

[18] Kates, R., Atkinson, D., Brant-Zawadzki, M. (1996). Fluid-attenuated inversion recovery (FLAIR): clinical prospectus of current and future applications. *Top Magn Reson Imaging*, 8: 389-96.

[19]Lanfermann, H., Heindel, W., Schaper, J., Schroder, R., Hansmann, M.L., Lehrke, R., Ernestus, I., & Lackner, K. (1997). CT and MR imaging in primary cerebral non-Hodgkin's lymphoma. *Acta Radiol, 38* (2): 259-67.

[20]Roman-Goldstein, S.M., Goldman, D.L., Howieson, J., Belkin, R., & Neuwelt, EA. (1992). MR of primary CNS lymphoma in immunologically normal patients. *AJNR Am J Neuroradiol, 13* (4): 1207-13.

[21]Bühring U., Herrlinger, U., Krings, T., Thiex, R., Weller, M. & Kuker, W. (2001). MRI features of primary central nervous system lymphomas at presentation. *Neurology, 57* (3): 393-6.

[22] Coulon, A., Lafitte, F., Hoang-Xuan, K., Martin-Duverneuil, N., Mokhtari, K., Blustajn, J., Chiras, J. (2002). Radiographic findings in 37 cases of primary CNS lymphoma in immunocompetent patients. *Eur Radiol, 12* (2): 329-40.

[23]Johnson, B.A., Fram, E.K., Johnson, P.C., Jacobowitz, R. (1997). The variable MR appearance of primary lymphoma of the central nervous system: comparison with histopathologic features. *AJNR Am J Neuroradiol*, *18* (3): 563-72.

[24] Kuker, W., Nagele, T., Korfel, A., et al. (2005). Primary central nervous system lymphomas (PCNSL): MRI features at presentation in 100 patients. *J Neurooncol, 72* (2): 169-177.

[25] Berger, J.R. (2003). Mass lesions of the brain in AIDS: the dilemmas of distinguishing toxoplasmosis from primary CNS lymphoma (2003). *AJNR Am J Neuroradiol, 24* (4): 554-5.

[26] Tan, B.R., & Bartlett, N.L. (2000). Treatment advances in non-Hodgkin's lymphoma. *Expert Opinion on Pharmacotherapy*, *1* (3): 451-65.

[27] Thomsen, C., Henriksen, O., & Ring, P. (1987). In vivo measurement of water self diffusion in the human brain by magnetic resonance. *Acta Radiol, 28*: 353-61.

[28] Einstein, A. Investigations on the theory of the Brownian movement. New York, NY: Dover, 1956.

[29] Hagmann, P., Jonasson, L., Maeder, P., Thiran, J.-P., Wedeen, V.J., & Meuli, R. (2006). Understanding diffusion MR imaging techniques: from scalar diffusion-weighted imaging to diffusion tensor imaging and beyond. *RadioGraphics, 26:* S205-S223.

[30] Hahn, E. (1950). Spin echoes. *Phys Rev, 80;* 580-94.

[31] Mori, S., & Barker, P.B. (1999). Diffusion magnetic resonance imaging: its principles and applications. *The Anatomical Record (New Anat.)*, *257*: 102-9.

[32] Woodward, P. (2001). *MRI for technologists.* New York: McGraw-Hill Medical. 408 pp.

[33] Stejskal, E.O. & Tanner, J.E. (1965). Spin diffusion measurements: spin-echo in the presence of a time dependent field gradient. *J Chem Phys, 42*: 288-92.

[34] Levitt, M.H. (2008). *Spin Dynamics: Basics of Nuclear Magnetic Resonance.* London: Wiley and Sons. 744 pp.

[35] Edelman, R.R., Wielopolski, P., Schmitt, F. (1994). Echo-planar MR imaging. *Radiology, 192*: 600-12.

[36] Le Bihan, D., Poupon, C., Amadon, A., & Lethimonnier, F. (2006). Artifacts and pitfalls in diffusion MRI. *J Magn Reson Imaging, 24* (3): 478-88.

[37] Le Bihan D., Breton, E., Lalemand, D., Grenier, P., Cabanis, E., & Laval-Jeantet, M. (1986). MR imaging of intravoxel incoherent motions: application to diffusion and perfusion in neurologic disorders. *Radiology, 161*: 401-07.

[38] Le Bihan, D. (2003). Looking into the functional architecture of the brain with diffusion MRI. *Nature Reviews Neuroscience, 4*: 469-80.

[39] Warach, S., Chien, D., Li, W., Ronthal, M., Edelman, R.R. (1992). Fast magnetic resonance diffusion-weighted imaging of acute human stroke. *Neurology 1992, 42:* 1717-1723.

[40] Moseley, M.E., Kucharczyk, J., Mintorovitch, J., Cohen, Y., Kurhanewicz, J., Derugin, N., Asgari, H., & Norman, D. (1990). Diffusion-weighted MR imaging of acute stroke: correlation with T2-weighted and magnetic susceptibility-enhanced MR imaging in cats. *AJNR Am J Neuroradiol, 11*: 423-429.

[41] Latour, L.L., Svoboda, K., Mitra, P.P., & Sotak, C.H. (1994). Time-dependent diffusion of water in a biological system. *Proc Natl Acad Sci USA, 91*: 1229-1233.

[42] Hossmann, K.-A., Fischer, M., Bockhorst, K., Hoehn-Berlage, M. (1994). NMR imaging of the apparent diffusion coefficient (ADC) for the evaluation of metabolic suppression and recovery after prolonged cerebral ischemia. *J. Cereb Blood Flow Metab., 14*: 723-731.

[43] Mintorovitch, J., Yang, G.Y., Shimizu, H., Kucharczyk, J., Chan, P.H., & Weinstein, P.R. (1994). Diffusion-weighted magnetic resonance imaging of acute focal cerebral ischemia: comparison of signal intensity with changes in brain water and Na+,K+-ATPase activity. *J. Cereb Blood Flow Metab, 14*: 723-31.

[44] Klatzo, I. (1987). Pathophysiological aspects of brain edema. *Acta Neuropathologica, 72* (3): 236-39.

[45] Knight, R.A., Ordidge, R.J., Helpern, J.A., Chopp, M., Rodolosi, L.C., & Peck, D. (1991). Temporal evolution of ischemic damage in rat brain measured by proton nuclear magnetic resonance imaging. *Stroke, 22*: 802-08.

[46] Marks, M.P. de Crespigny, A., Lentz, D., Enzmann, D.R., Albers, G.W., & Moseley, M.E. (1996). Acute and chronic stroke: navigated spin-echo diffusion-weighted MR imaging. *Radiology, 199*: 403-08.

[47] Provenzale, J.M. & Sorensen, A.G. (1999). Diffusion-weighted MR imaging in acute stroke: theoretic considerations and clinical applications. *AJR Am J Roentgenol, 173* (6): 1459-67.

[48] Albers, G.W., Lansberg, M.G., Norbash, A.M., Tong, D.C., O'Brien, M.W., Woolfenden, A.R., Marks, M.P., & Moseley, M.E. (2000). Yield of diffusion-weighted MRI for detection of potentially relevant findings in stroke patients. *Neurology, 54*: 1562-67.

[49] Bodini, B., & Ciccarelli, O. (2009). Diffusion MRI in neurological disorders. In H. Johansen-Berg & T. E.J. Behrens (Eds.), *Diffusion MRI: From quantitative*

measurement to in vivo neuroanatomy (176-194). London: Elsevier Academic Press.

[50] Paviour, D.C., Thornton, J.S., Lees, A.J. & Jager, H.R. (2006). Diffusion-weighted magnetic resonance imaging differentiates Parkinsonian variant of multiple-system atrophy from progressive supranuclear palsy. *Movement Disorders, 22* (1): 68-74.

[51] Schocke, M.F.H., Seppi, K., Esterhammer, R., Kremser, C., Jaschke, W., Poewe, W., & Wenning, G.K. (2002). Diffusion-weighted MRI differentiates the Parkinson variant of multiple system atrophy from PD. *Neurology, 58:* 575-580.

[52] Hanyu, H., Asano, T., Sakurai, H., Imon, Y., Iwamoto, T., Takasaki, M., Shindo, H., & Abe, K. (1999). Diffusion-weighted and magnetization transfer imaging of the corpus callosum in Alzheimer's disease. *Journal of the Neurological Sciences, 1* (1): 37-44.

[53] Shiga, Y., Miyazawa, K. Sato, S., Fukushima, R., Shibuya, S., Sato, Y., Konno, H., Doh-ura, K., Mugikura, S., Tamura, H., Higano, S., Takahashi, S., & Itoyama, Y. (2004). Diffusion-weighted MRI abnormalities as an early diagnostic marker for Creutzfeldt-Jakob disease. *Neurology, 63*: 443-49.

[54] Rovaris, M., Gass, A., Bammer, R., Hickman, S.J., Ciccarelli, O., Miller, D.H., & Fillippi, M. (2005). Diffusion MRI in multiple sclerosis. *Neurology*, *65*: 1526-36.

[55] Tsuchiya, K., Katase, S., Yoshino, A., Hachiya, J. (1999). Diffusion-weighted MR imaging of encephalitis. *Am J Radiol, 173:* 1097-99.

[56] Yogarajah, M. & Duncan, J.S (2007). Diffusion-based magnetic resonance imaging and tractography in epilepsy. *Epilepsia, 49* (2): 189-200.

[57] Tsuruda, S.J., Chew, M.W., Moseley, E.M., & Norman, D. (1990). Diffusion-weighted MR imaging of the brain: value of differentiating between extra axial cysts and epidermoid tumors. *AJNR Am J Neuroradiol, 11*: 925-31.

[58] Lai, P.H., Ho, J.T., Chen, W.L., Hsu, S.S., Wang, J.S., Pan, H.B., & Yang, C.F. (2002). Brain abscess and necrotic brain tumor: discrimination with proton MR spectroscopy and diffusion-weighted imaging. *AJNR Am J Neuroradiol, 23:* 1369-77.

[59] Koh, D.M., & Padhani, A.R. (2006). Diffusion-weighted MRI: a new functional clinical technique for tumour imaging. *Br J Radiol, 79* (944): 633-5.

[60] Pauleit, D., Langen K.-J., Floeth, F., Hautzel, H., Riemenschneider, M.J., Reifenberger, G., Shah, N.J., & Muller, H.-W. (2004). Can the apparent diffusion coefficient be used as a noninvasive parameter to distinguish tumor tissue from peritumoral tissue in cerebral gliomas?. *J Magn Reson Imaging, 20* (5): 758-64.

[61] Bulakbasi, N., Guvenc, I., Onguru, O., Erdogan, E., Tayfun, C., & Ucoz, T. (2004). The added value of the apparent diffusion coefficient calculation to magnetic resonance imaging in the differentiation and grading of malignant brain tumors. *J Comput Assist Tomogr, 28* (6): 735-46.

[62] Kono, K., Inoue, Y., Nakayama, K., Shakudo, M., Morino, M., Ohata, K., Wakasa, K., & Yamada, R. (2001). The role of diffusion-weighted imaging in patients with brain tumors. *AJNR Am J Neuroradiol, 22* (6): 1081-8.

[63] Tien, R.D., Felsberg, G.J., Friedman, H., Brown, M., & MacFall, J. (1994). MR imaging of high-grade cerebral gliomas: value of diffusion-weighted echo planar pulse sequences. *AJR Am J Roentgenol, 162*: 671-77.

[64] Castillo, M., Smith, J.K., Kwock, L., & Wilber, K. (200). Apparent diffusion coefficients in the evaluation of high-grade cerebral gliomas. *AJNR Am J Neuroradiol*, *22*: 60-4.

[65] Stadnik, T.W., Chaskis, C., Michotte, A., Shabana, W.M., van Rompaey, K., Luypaert, R., Budinsky, L., Jellus, V., Osteaux, M. (2001). Diffusion-weighted MR imaging of intracerebral masses: comparison with conventional MR imaging and histologic findings. *AJNR Am J Neuroradiol, 22* (5): 969-76.

[66] Zimmerman, R.D. (2001). Is there a role for diffusion-weighted imaging in patients with brain tumors or is the "bloom off the rose"?. *AJNR Am J Neuroradiol*, *22* (6): 1013-4.

[67] Zacharia, T.T., Law, M., Naidich, T.P., & Leeds, N.E. (2008). Central nervous system lymphoma characterization by diffusion-weighted imaging and MR spectroscopy. *J Neuroimaging, 18* (4): 411-17.

[68] Reiche, W., Hagen, T., Schuchardt, V., & Billmann, P. (2007). Diffusion-weighted MR imaging improves diagnosis of CNS lymphomas. A report of four cases with common and uncommon imaging features. *Clin Neurol Neurosurg , 109* (1): 92-101.

[69] Guo, A.C., Cummings, T.J., Dash, R.C., & Provenzale, J.M. (2002). Lymphomas and high-grade astrocytomas: comparison of water diffusibility and histologic characteristics. *Radiology, 224* (1): 177-83.

[70] Yamasaki, F., Kurisu, K., Satoh, K., Arita, K., Sugiyama, K., Ohtaki, M., Takaba, J., Tominaga, A., Hanaya, R., Yoshioka, H., Hama, S., Ito, Y. Kajiwara, Y., Yahara, K., Saito, T., & Thohar, M. (2005). Apparent diffusion coefficient of human brain tumors at MR imaging. *Radiology, 235* (3): pp. 985-91

[71]Toh, C._H., Castillo, M., Wong, A. M.-C., Wei, K.-C., Wong, H.-F., Ng, S.-H., & Wan, Y.-L. (2008). Primary cerebral lymphoma and glioblastoma multiforme: differences in diffusion characteristics evaluated with diffusion tensor imaging. *AJNR Am J Neuroradiol, 29* (3): 471-5.

[72] Horger, M., Fenchel, M., Nagele, T., Moehle, R., Claussen, C.D., Beschorner, R., & Ernemann, U (2009). Water diffusivity: comparison of primary CNS lymphoma and astrocytic tumor infiltrating the corpus callosum. *AJR Am J Roentgenol 193* (5): 1384-7.

[73] Calli, C., Kitis, O., Yunten, N., Yurtseven, T., Islekel, S., & Akalin, T. (2006). Perfusion and diffusion MR imaging in enhancing malignant cerebral tumors. *Eur J Radiol, 58* (3): 394-403.

[74] Al-Okaili, R.N., Krejza, J., Woo, J.H., Wolf, R.L., O'Rourke, D.M., Judy, K.D., Poptani, H., & Melhem, E.R. (2007). Intraaxial brain masses: MR imaging-based diagnostic strategy--initial experience. *Radiology*, *243* (2): 539-50.

[75] Barajas, R.F., Rubenstein, J.L., Chang, J.S., Hwang, J., & Cha, S. (2010). Diffusion-Weighted MR Imaging Derived Apparent Diffusion Coefficient Is Predictive of Clinical Outcome in Primary Central Nervous System Lymphoma. *AJNR Am J Neuroradiol*, *31* (1): 60-66.

[76] Server, A., Kulle, B., Maehlen, J., Josefsen, R., Schellhorn, T., Kumar, T., Langberg, C.W., & Nakstad, P.H. (2009). Quantitative apparent diffusion coefficients in the characterization of brain tumors and associated peritumoral edema. *Acta Radiol, 50* (6): 682-9.

[77] Okamoto, K., Ito, J., Ishikawa, K., Sakai, K., & Tokiguchi, S. (2000). Diffusion-weighted echo-planar MR imaging in differential diagnosis of brain tumors and tumor like conditions. *Eur Radiol*, 10 (8): 1342-50.

[78] Sadeghi, N., Camby, I., Goldman, S., Gabius, H.-J., Baleriaux, D., Salmon, I., Decaesteckere, C., Kiss, R., & Metens, T. (2003). Effect of hydrophilic components of the extracellular matrix on quantifiable diffusion-weighted imaging of human gliomas: preliminary results of correlating apparent diffusion coefficient values and hyaluronan expression level. *AJR Am J Roentgenol, 181 (1)*: 235-41.

[79] Akter, M., Hirai, T., Makino, K., Kitajima, M., Murakami, R., Fukuoka, H., Sasao, A., Kuratsu, J.I., & Yamashita, Y. (2008). Diffusion-weighted imaging of primary brain lymphomas: effect of ADC value and signal intensity of T2-weighted imaging. *Comput Med Imaging Graph, 32 (7)*: 539-43.

[80] DeAngelis LM. Cerebral lymphoma presenting as nonenhancing lesion on computed tomographic/magnetic resonance scan. *Ann Neurol.* 1993;33:308-311.

[81] Kitis, O., Altay, H., Calli, C., Yunten, N., Akalin, T. & Yurtseven, T. (2005). Minimum apparent diffusion coefficients in the evaluation of brain tumors. *Eur J Radiol, 55 (3)*: 393-400

[82] Camacho, D.L.A., Smith, J.K., Castillo, M. (2003). Differentiation of toxoplasmosis and lymphoma in AIDS patients by using apparent diffusion coefficients. *AJNR Am J Neuroradiol, 24* (4): 633-7.

[83] Burdette, J.H., Elster, A.D., & Ricci, P.E. (1998). Calculation of apparent diffusion coefficients (ADCs) in brain using two-point and six-point methods. *J Comput Assist Tomogr., 22(5):* 792-4.

[84] Provenzale, J.M., Mukundan, S., & Barboriak, D.P. (2006). Diffusion-weighted and perfusion MR imaging for brain tumor characterization and assessment of treatment response. *Radiology, 239(3):* 632-49.

[85] Koeller, K.K., Smirnitopoulos, J.G., & Jones, R.V. (1997). Primary central nervous system lymphoma: radiologic-pathologic correlation. *RadioGraphics,* 17: 1497-1526.

[86] Burstein, S.D., Kernohan, J.W., & Uihlein, A. (1963). Neoplasms of the reticuloendothelial system of the brain. *Cancer,* 16: 289-305.

[87] Asao, C., Korogi, Y., Kitajima, M., Hirai, T., Baba, Y., Makino, K., Kochi, M., Morishita, S., & Yamashita, Y. (2005). Diffusion-weighted imaging of radiation-induced brain injury for differentiation from tumor recurrence. *AJNR Am J Neuroradiol, 26*: 1455-60.

[88] Al Sayyari, A., Buckely, R., McHenery, C., Pannek, K., Coulthard, A., & Rose, S. (2010). Distinguishing recurrent primary brain tumor from radiation injury: a preliminary study using a susceptibility-weighted MR imaging-guided apparent diffusion coefficient strategy. *AJNR Am J Neuroradiol.*

[89] Smith, J.S., Cha, S., Mayo, M.C., McDermott, M.W., Parsa, A.T., Chang, S.M., Dillon, W.P., & Berger, M.S. (2005). Serial diffusion-weighted magnetic resonance imaging in cases of glioma: distinguishing tumor recurrence from postresection injury. *J Neurosurg, 103(3)*: 428-38.

[90] Chenevert, T.L., Stegman, L.D., Taylor, J.M., Robertson, P.L., Greenberg, H.S., Rehemtulla, A., Ross, B.D. (2000). Diffusion magnetic resonance imaging: an early surrogate marker for therapeutic efficacy in brain tumors. *J Natl Cancer Inst.* 2000, 92(24): 2029-36.

[91] Jain, R., Scarpace, L.M., Ellika, S., Torcuator, R., Schultz, L.R., Hearshen, D., & Mikkelsen, T. (2010). Imaging response criteria for recurrent gliomas treated with

bevacizumab: role of diffusion weighted imaging as an imaging biomarker. *J Neuroncol., 96(3):* 423-31.

[92] Mardor, Y., Pfeffer, R., Spiegelmann, R., Roth, Y., Maier, S.E., Nissim, O., Berger, R., Glicksman, A., Baram, J., Orenstein, A., & Cohen, J.S. (2003). Early detection of response to radiation therapy in patients with brain malignancies using conventional and high b-value diffusion-weighted magnetic resonance imaging. *Journal of Clinical Oncology, 21* (6): 1094-1100.

[93] Mardor, Y., Roth, Y., Lidar, Z., Jonas, T., Pfeffer, R., Maier, S.E., Meir, F., Nass, D., Hadani, M., Orenstein, A., Cohen, J.S., & Ram, Z. (2001). Monitoring response to convection-enhanced taxol delivery in brain tumor patients using diffusion-weighted magnetic resonance imaging. *Cancer Research, 61*: 4971-73.

[94] Ellingson, B.M., Rand, S.D., Malkin, M.G., & Schmainda, K.M. (2010). Utility of functional diffusion maps to monitor a patient diagnosed with gliomatosis cerebri. *J Neuroncol., 97 (3):* 419-23.

[95] Moffat, B.A., Chenevert, T.L., Lawrence, T.S., Meyer, C.R., Johnson, T.D., Dong, Q., Tsien, C., Mukherji, S., Quint, D.J., Gebarski, S.S., Robertson, P.L., Junck, L.R., Rehemtulla, A., & Ross, B.D. (2005). Functional diffusion map: a noninvasive MRI biomarker for early stratification of clinical brain tumor response. *Proc Natl Acad Sci U S A., 102 (15)*: 5524-9.

[96] Hamstra, D.A., Galban, C.J., Meyer, C.R., Johnson, T.D., Sundgren, P.C., Tsien, C., Lawrence, T.S., Junck, L., Ross, D.J., Rehemtulla, A., Ross, B.D., & Chenevert, T.L. (2008). Functional diffusion map as an early imaging biomarker for high-grade glioma: correlation with conventional radiologic response and overall survival. *J Clin Oncol, 26(20)*: 3387-94.

[97] Moseley, M.E., Cohen, Y., Kucharczyk, J., Mintorovitch, J., Asgari, H.S., Wendland, M.F., Tsuruda, J., & Norman, D. (1990). Diffusion-weighted MR imaging of anisotropic water diffusion in cat central nervous system. *Radiology,* 176: 439-45.

[98] Chenevert, T.L., Brunberg, J.A.,& Pipe, J.G. (1990). Anisotropic diffusion in human white matter: demonstration with MR techniques in vivo. *Radiology, 177*: 401-05.

[99] Stadlbauer, A., Ganslandt, O., Buslei, R., Hammen, T., Gruber, S., Moser, E., Buchfelder, M., Salomonowitz, E., & Nimsky, C. (2006). Gliomas: histopathologic evaluation of changes in directionality and magnitude of water diffusion at diffusion-tensor MR imaging. *Radiology, 240*: 803-10.

APPENDIX – MR IMAGING DATA

Case 1

ADC

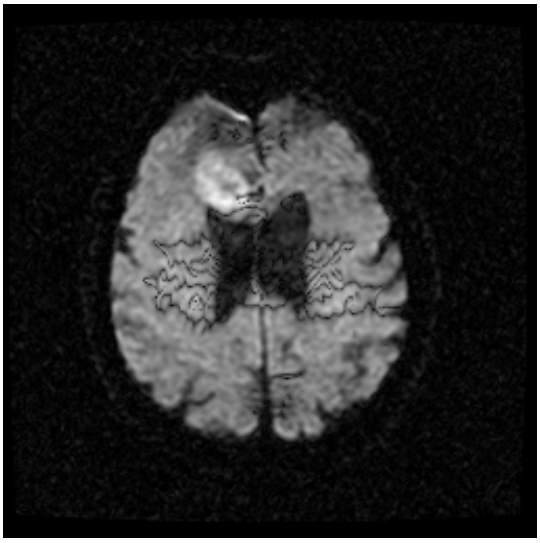

DWI

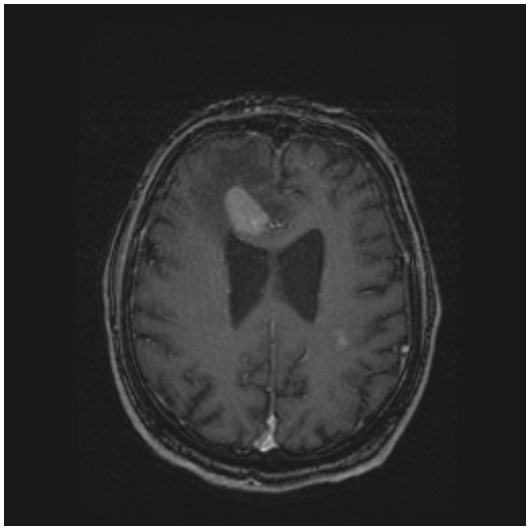

Axial IR/SPGR post

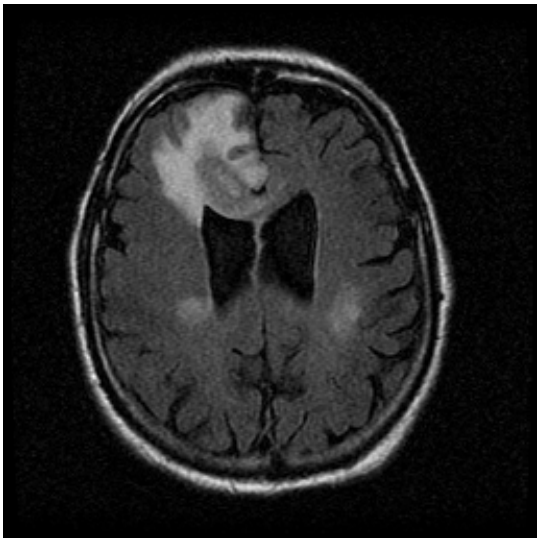

Axial FLAIR

Case 2

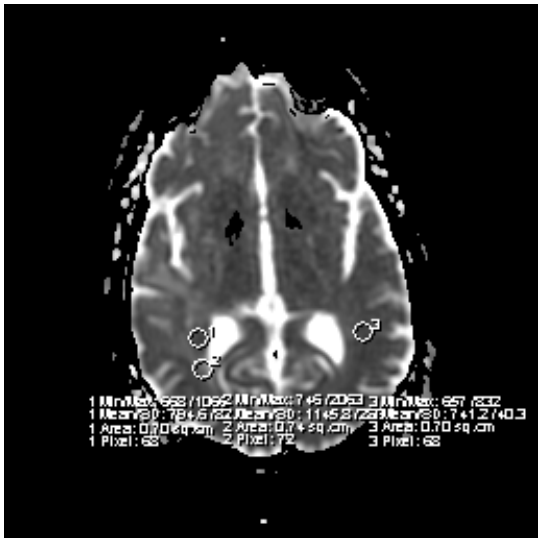

ADC

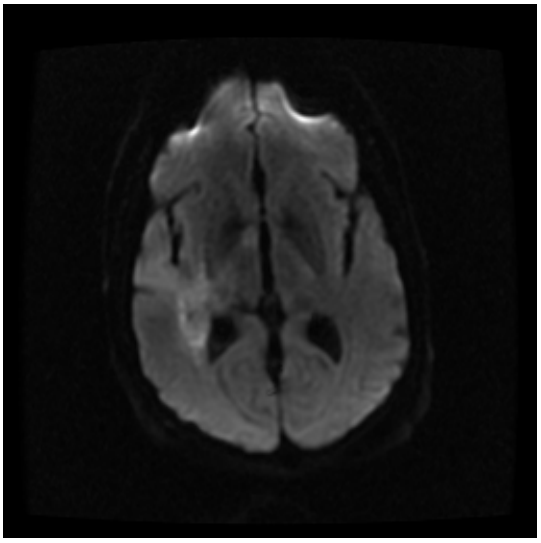

DWI

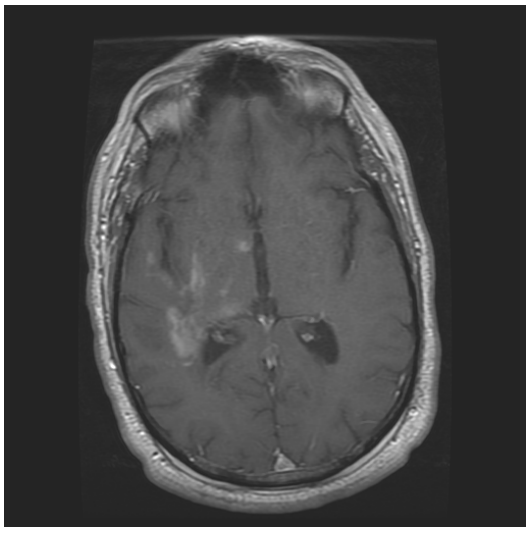

Axial IR/SPGR post

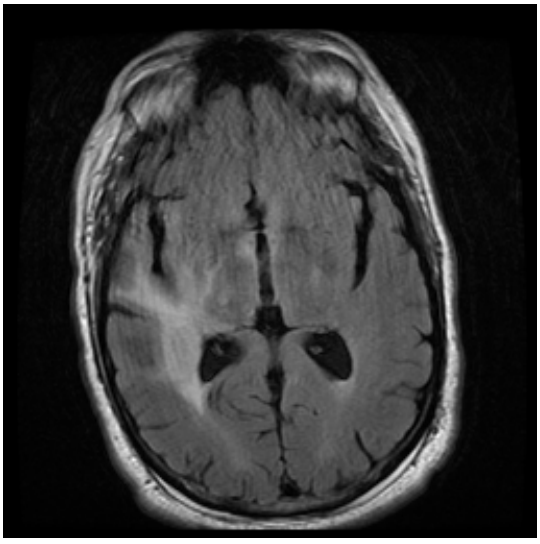

Axial FLAIR

Case 3

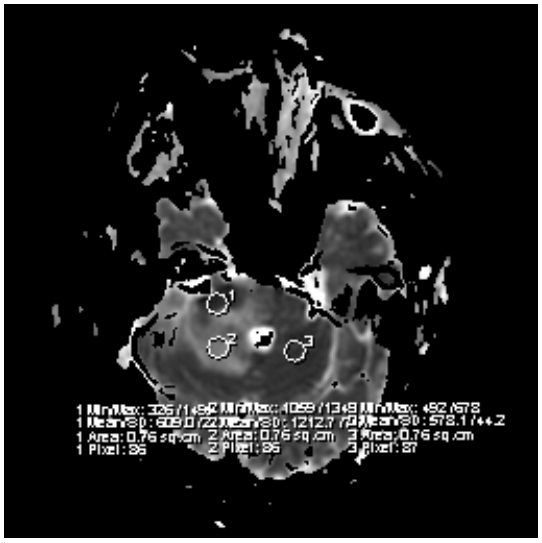

ADC

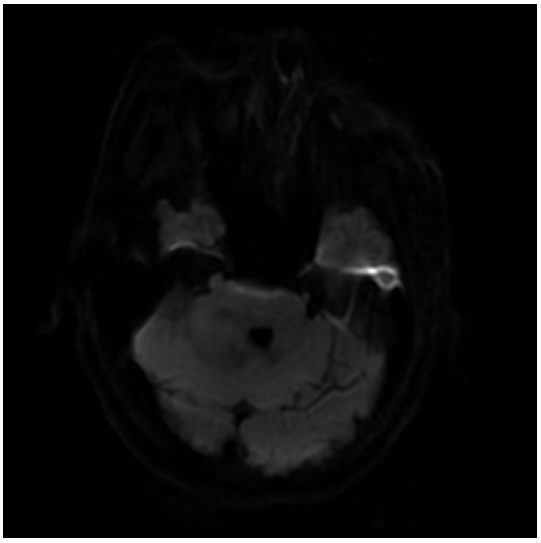

DWI

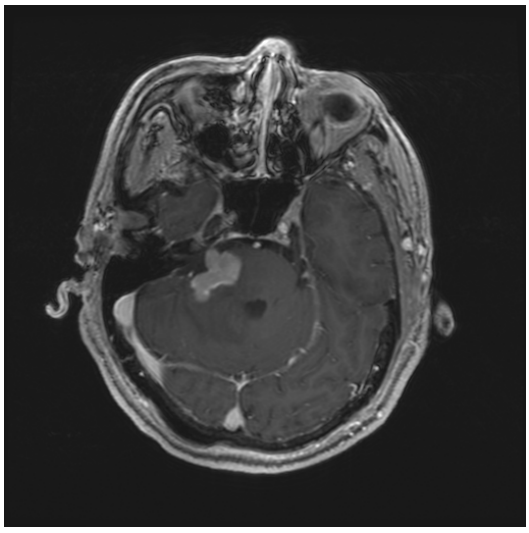

Axial IR/SPGR post

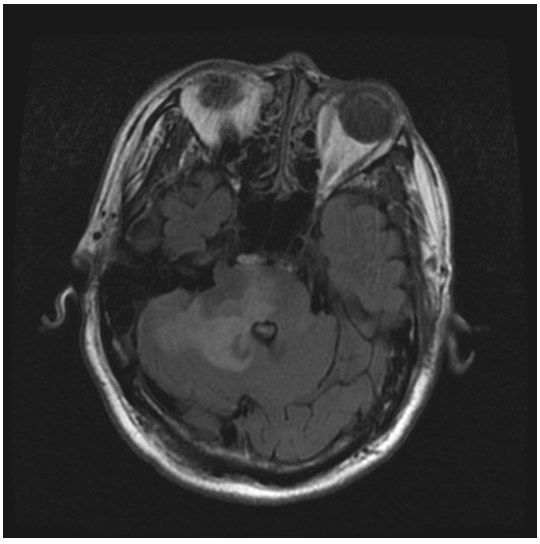

Axial FLAIR

Case 4

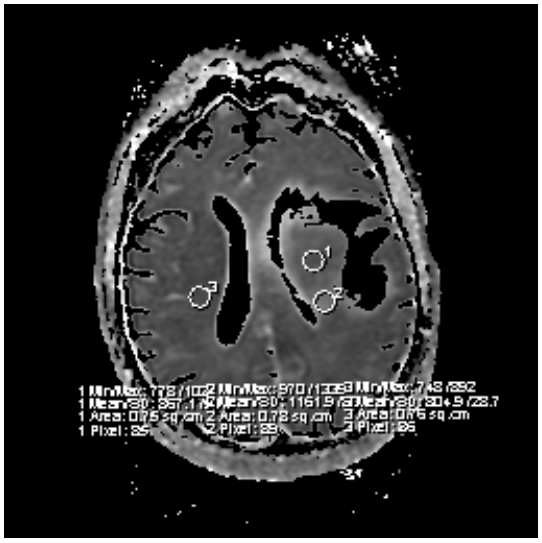

ADC

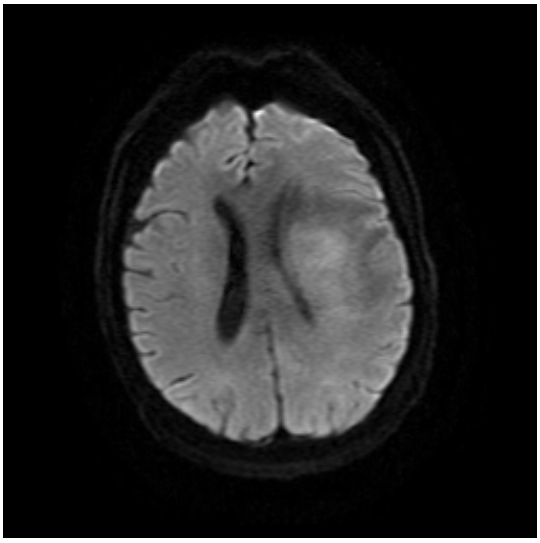

DWI

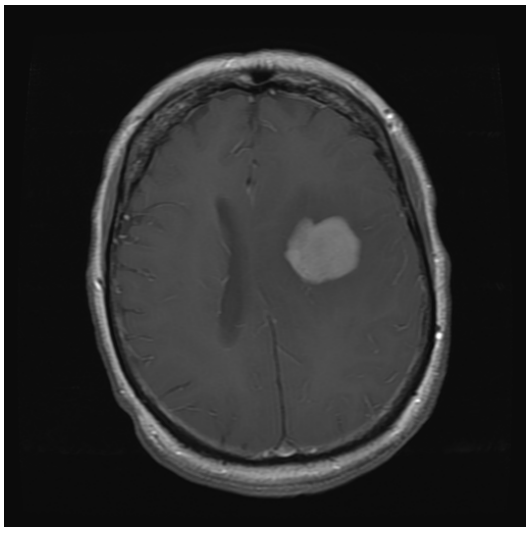

Axial IR/SPGR post

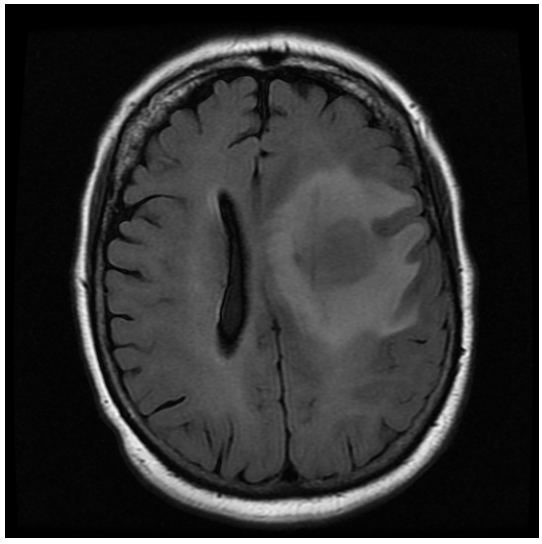

Axial FLAIR

Case 5

ADC

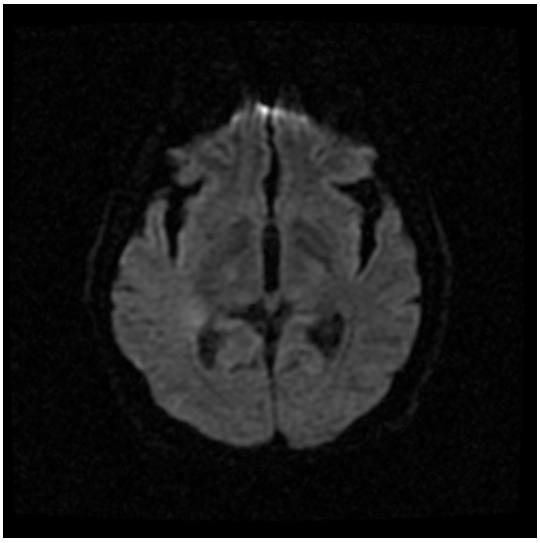

DWI

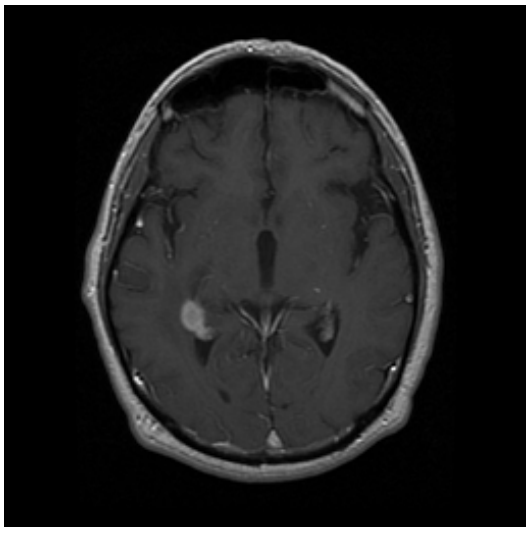

Axial IR/SPGR post

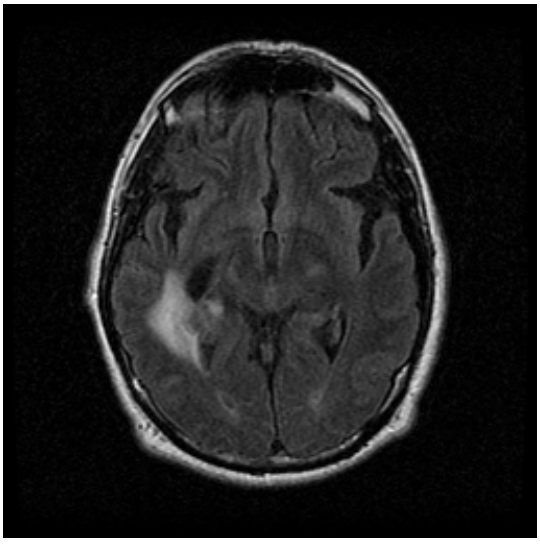

Axial FLAIR

Case 6

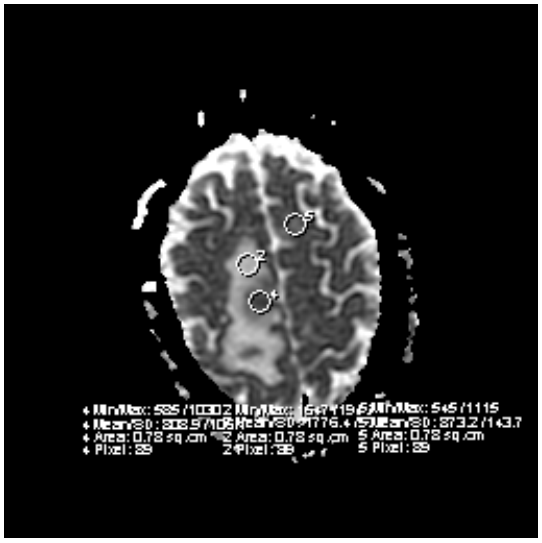

ADC

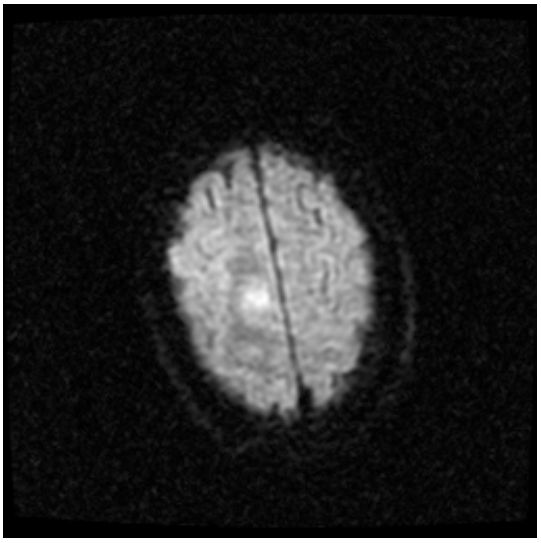

DWI

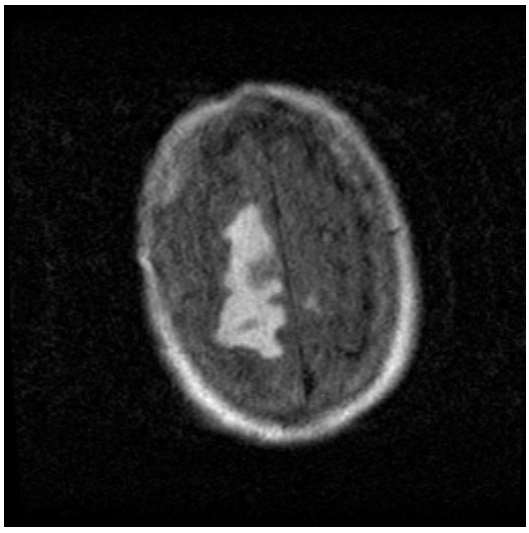

Axial FLAIR

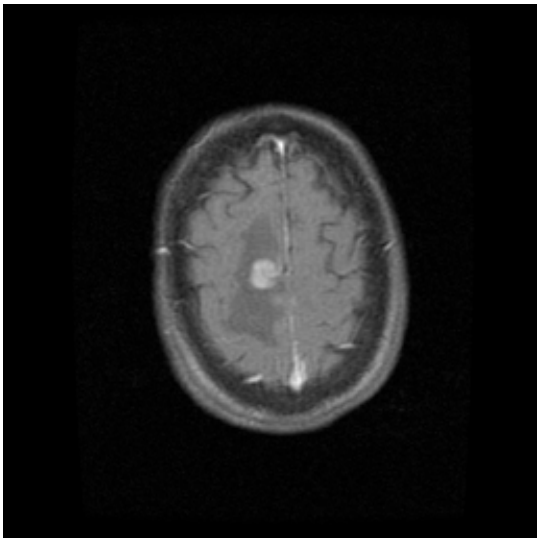

Axial IR/SPGR post

Case 7

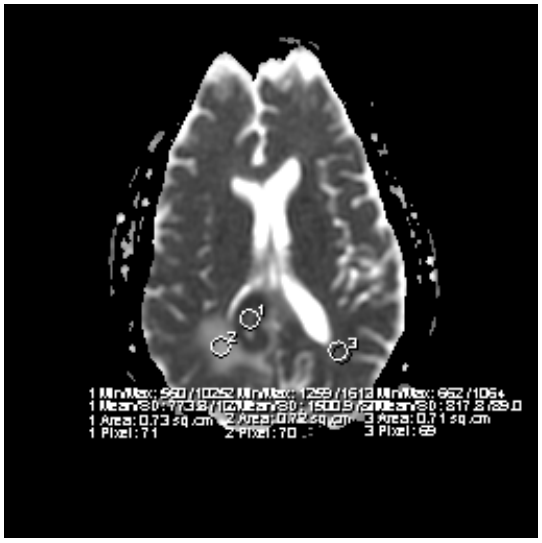

ADC

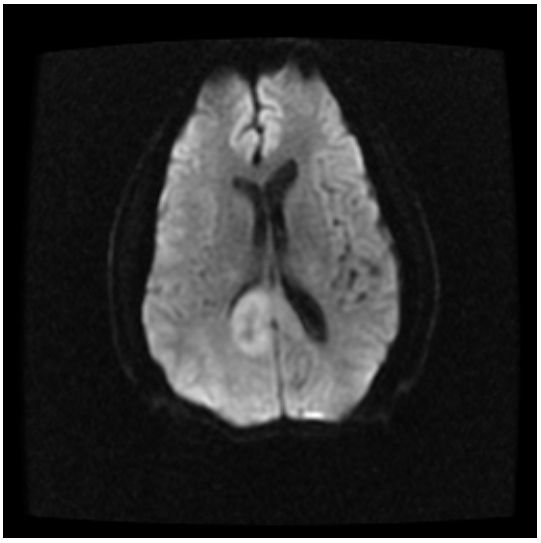

DWI

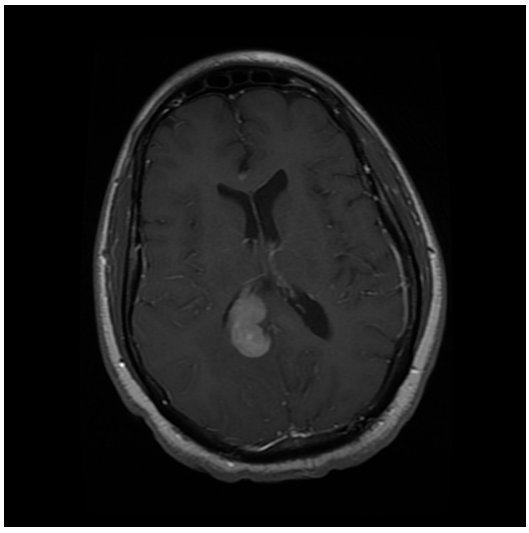

Axial IR/SPGR post

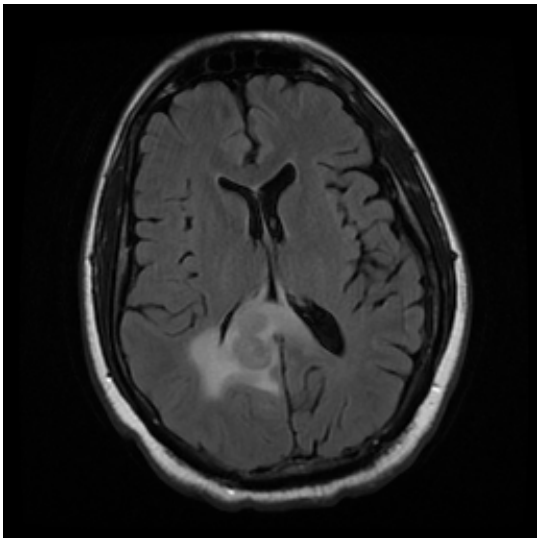

Axial FLAIR

Case 8 – lesion ROI

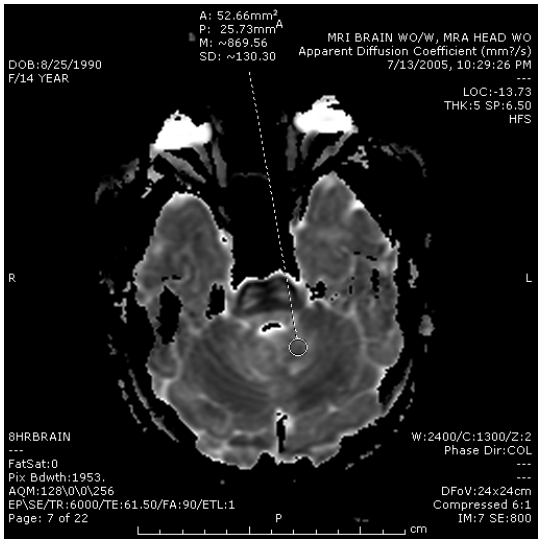

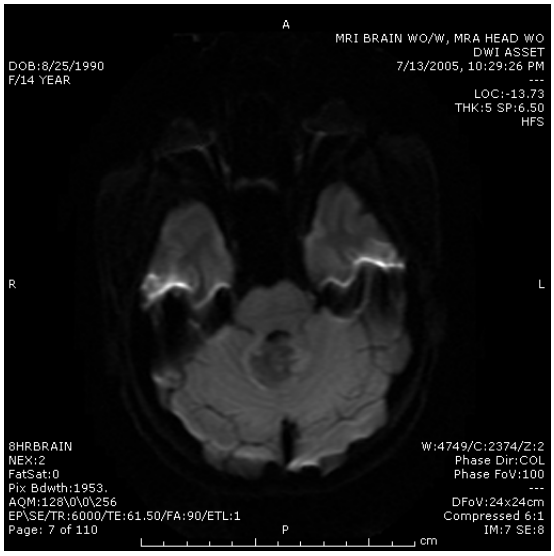

ADC-lesion DWI-lesion

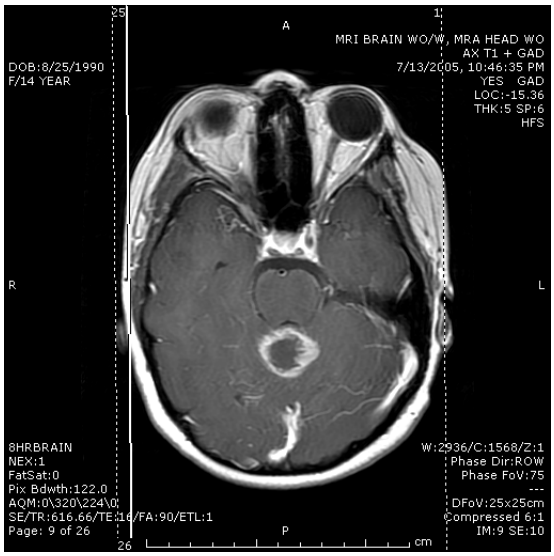

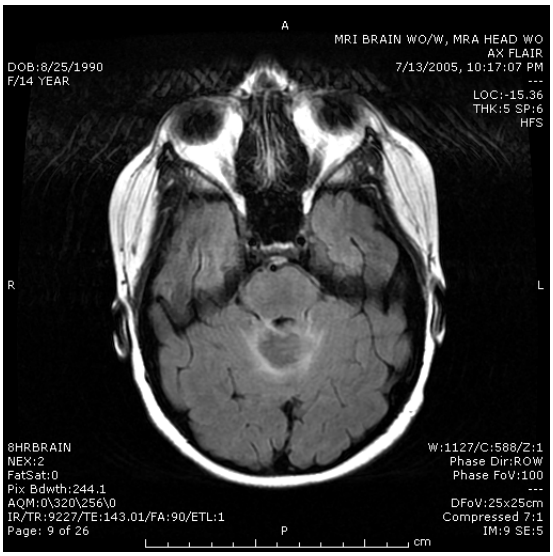

Axial IR/SPGR post-lesion Axial FLAIR-lesion

Case 8- perifocal ROI

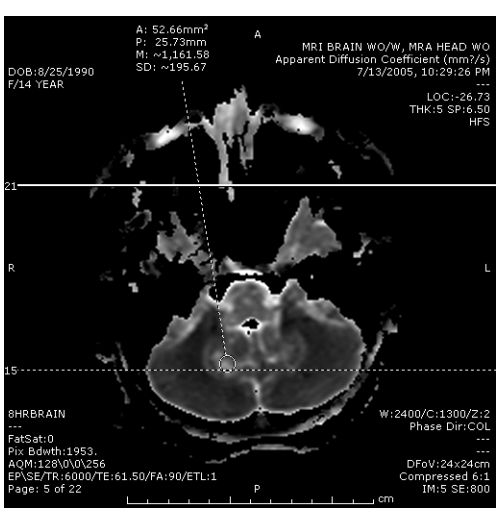

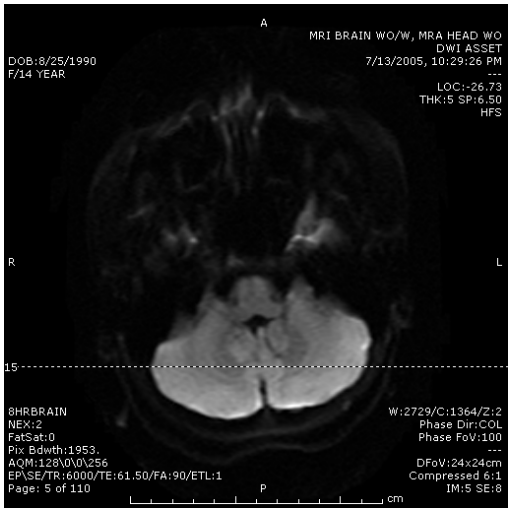

ADC-perifocal

DWI-perifocal

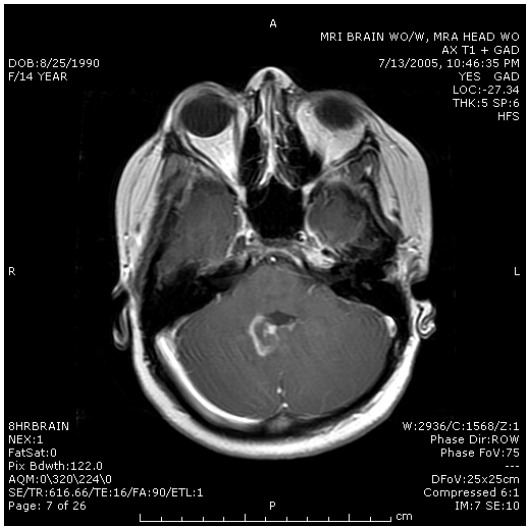

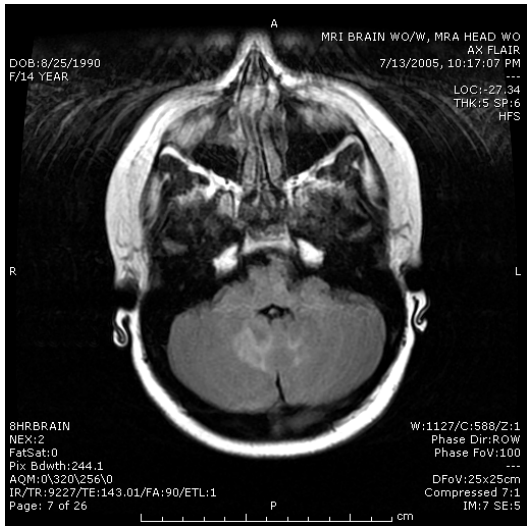

Axial IR/SPGR perifocal

Axial FLAIR- perifocal

Case 8 – normal ROI

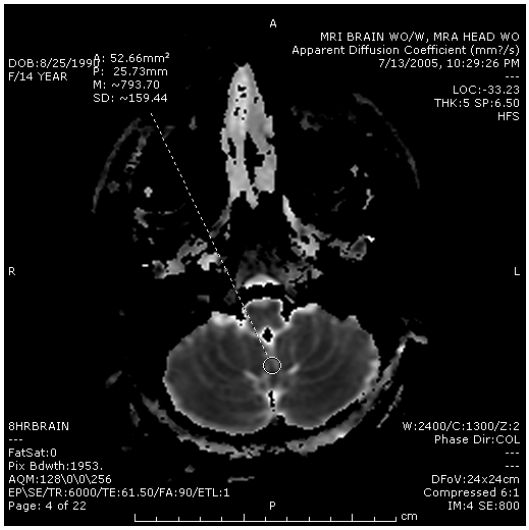

ADC-normal

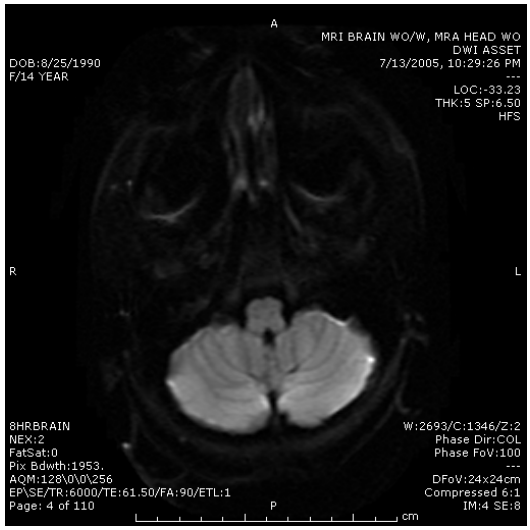

DWI-normal

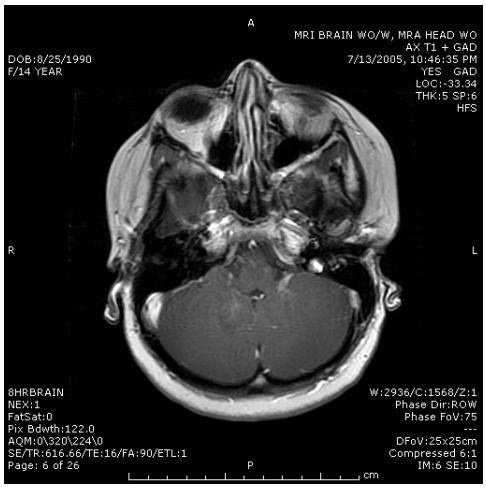

Axial IR/SPGR normal

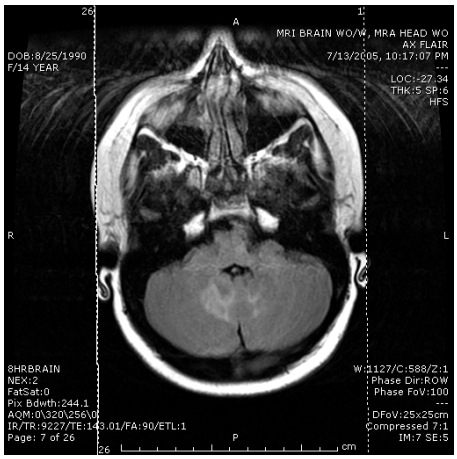

Axial FLAIR- normal

Case 9

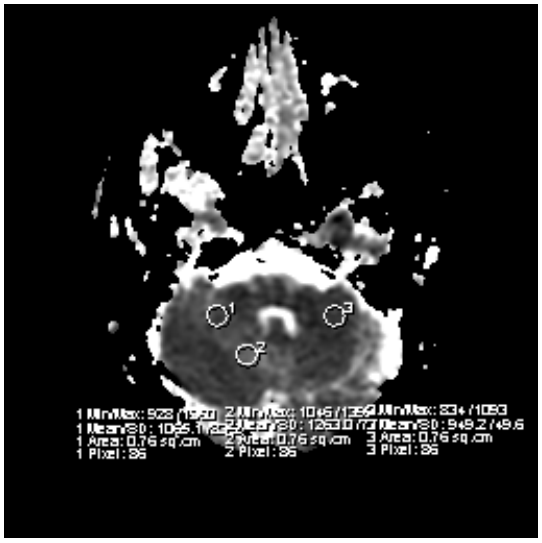

ADC

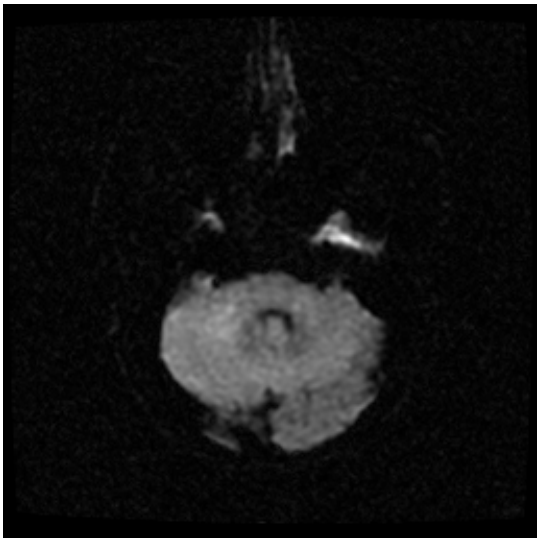

DWI

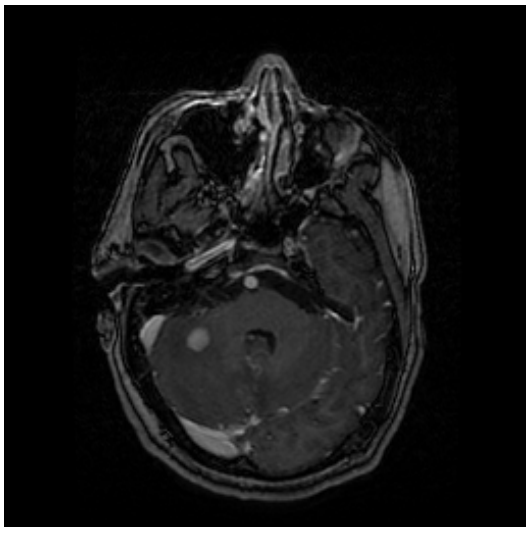

Axial IR/SPGR post

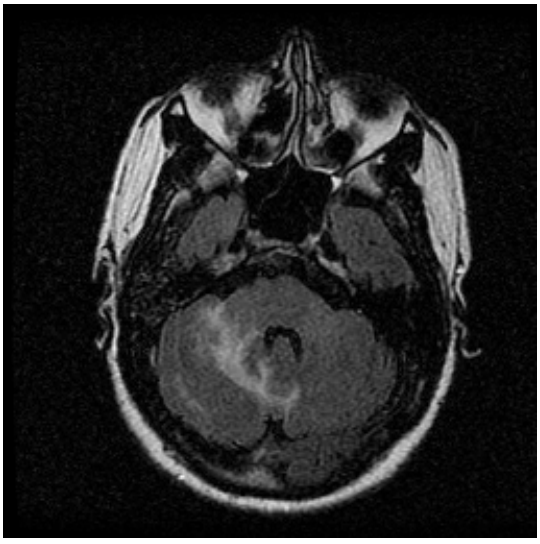

Axial FLAIR

Case 10

ADC

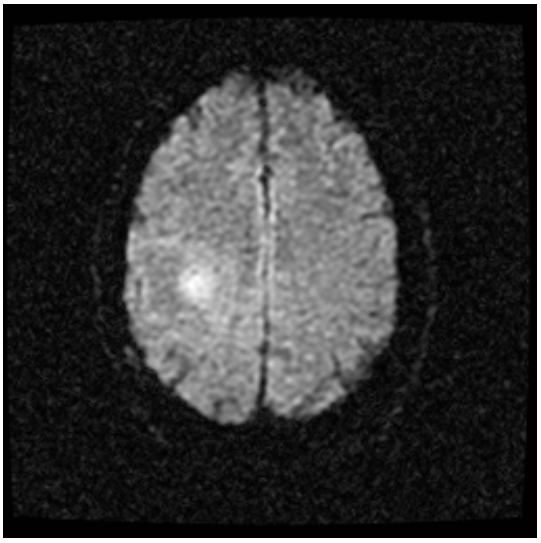

DWI

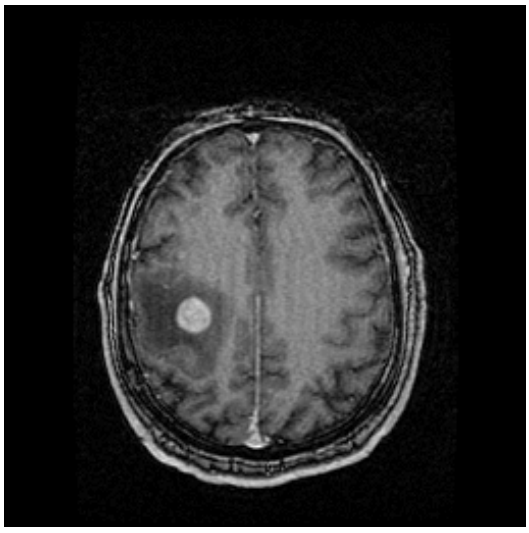

Axial IR/SPGR post

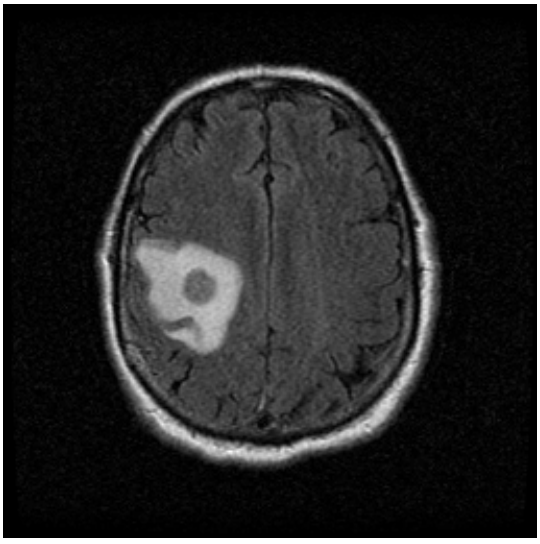

Axial FLAIR

Case 11

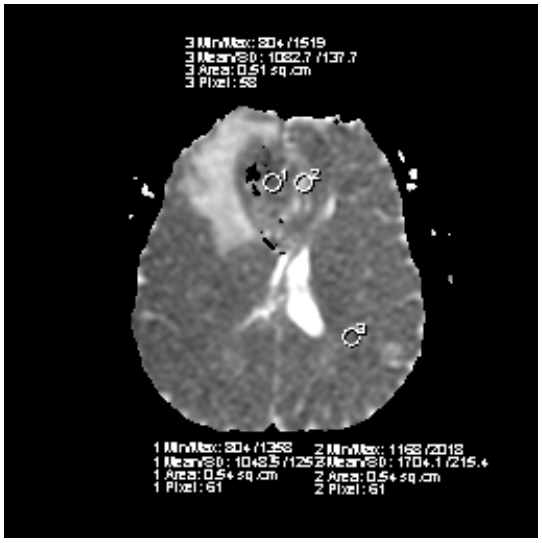

ADC

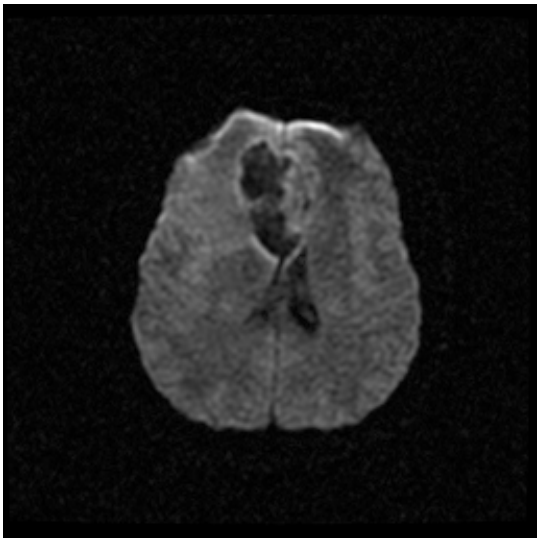

DWI

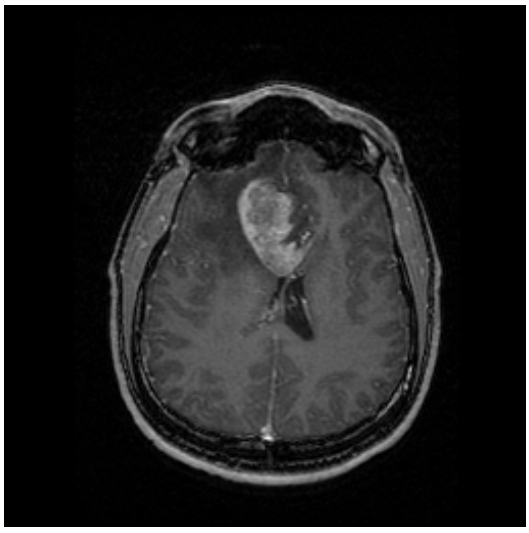

Axial IR/SPGR post

Axial FLAIR

Case 12

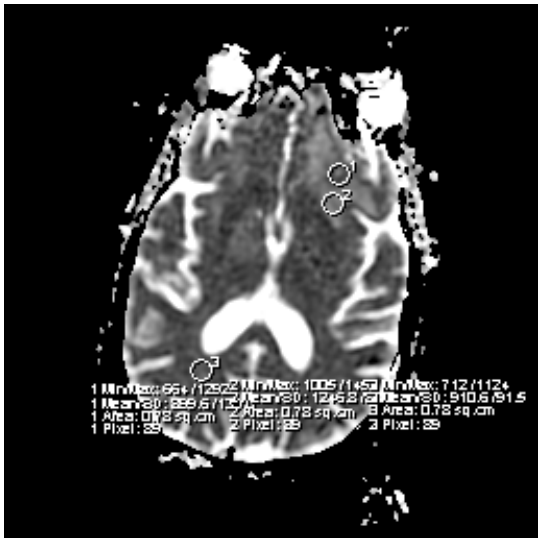

ADC

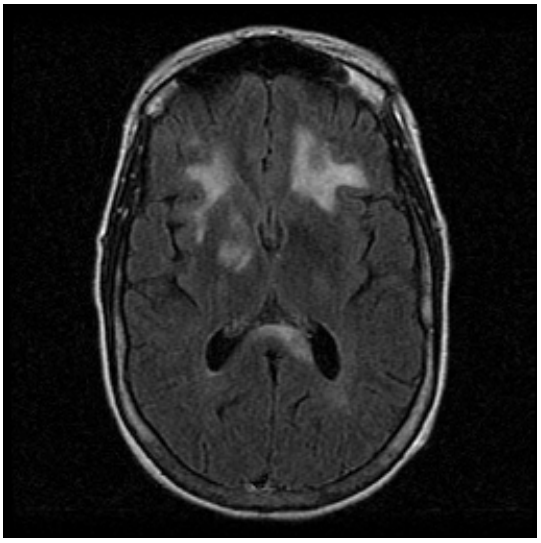

DWI

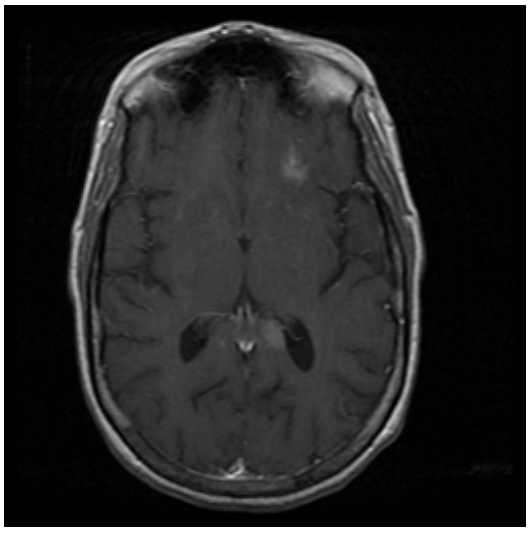

Axial IR/SPGR post

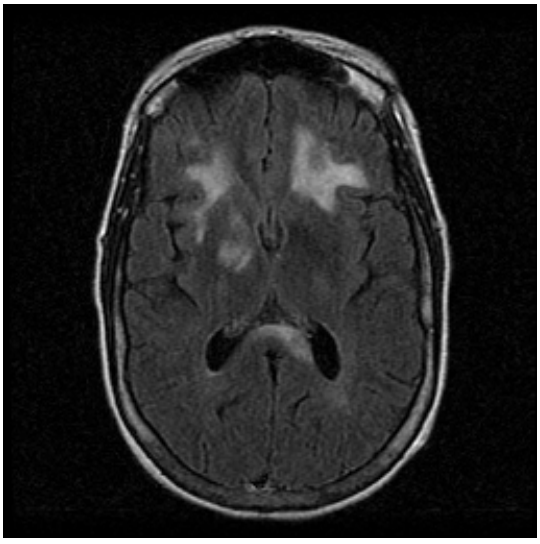

Axial FLAIR